Research Article

Daniel T. Filipovic* and Gerald R. Kress

Free-edge effects of corrugated laminates

https://doi.org/10.1515/cls-2020-0009
Received May 27, 2020; accepted Jul 16, 2020

Abstract: Due to their high numerical efficiency, homogenization models are often employed in the analysis of corrugated laminates. They are usually derived assuming periodic behavior in the corrugated direction and generalized plane strain in the out-of-plane direction, which corresponds to the assumption of infinite dimensions of the structure. As a consequence, any influences of edge effects are not mapped, although they can have a significant impact on the mechanical behavior of a given structure. The objective of this manuscript is to investigate the influence of boundary conditions - a combination of free-edges and clamping - on the structural stiffness of corrugated laminates. A total of six load cases are investigated which correspond to the line loads considered in the classical theory of laminated plates. The results of this parameter study allow the identification of several critical loading situations, where free edges can significantly alter structural stiffness. The given investigations hence contribute to the investigation of the validity range of homogenization models.

Keywords: corrugated laminate, composite materials, free-edge effects

1 Introduction

The geometric effects of cylindrical corrugations can create highly anisotropic structural properties with respect to in-plane extension or bending of corrugated sheets. Decades ago, corrugated metal sheets were used for airplane design, were the local bending stiffness of the corrugations replaces the ribs (wing) or stringers (fuselage) to increase buckling strength [1–4]. The book by Mornement and Holloway describes use of corrugated iron in civil engineering [5]. During recent decades, the increasing research interest in corrugated laminates has been motivated by a range of applications as well as by modeling challenges.

1.1 General investigations of corrugated laminates

Thurnherr et al. have investigated interlaminar stress in corrugated laminates [6]. The geometrically nonlinear behavior of corrugated laminates was studied by Thurnherr et al. [7, 8], Bai et al. [9], Kress and Filipovic [10] and by Soltani et al. [11]. The peculiar vibration behavior of corrugated laminates was studied by Thurnherr et al. [12], Malikan et al. [13] and by Nguyen et al. [14]. A planar FEM formulation for simulating the response of corrugated laminates to transverse shear line force was developed by Filipovic and Kress [15]. The question of how to manufacture high-amplitude corrugated laminates with circular-sections corrugation shape was addressed by Filipovic and Kress [16].

1.2 Applications

The review by Dayyani et al. [17] considers a range of applications as well as the mechanical behavior of composite corrugated structures.

1.2.1 Flexible skin in morphing-wing design

The morphing wing can change its airfoil shape without using the current-technology rigid flaps and slats [18]. Potential advantages of the concept include savings of mass and reduction of the number of parts as well as improved flight-mission performance [19]. A review of modeling and analysis of morphing wings was given by Li et al. [20]. Thill et al. [21] gave a review dedicated to the subject of morphing skins. Some morphing-wing design concepts call for sections of flexible skin, that should contribute to the wing-skin stiffness along the span and have high compliance and deformability along the chord directions where early design studies were performed by Thill et al. [22] and by Ghandi and Anusonthi [23]. A literature survey on com-

*Corresponding Author: Daniel T. Filipovic: Laboratory of Composite Materials and Adaptive Structures, Department of Mechanical and Process Engineering, ETH Zürich, Tannenstr. 3, CH-8092 Zürich, Switzerland; Email: fidaniel@ethz.ch
Gerald R. Kress: Laboratory of Composite Materials and Adaptive Structures, Department of Mechanical and Process Engineering, ETH Zürich, Tannenstr. 3, CH-8092 Zürich, Switzerland

posite corrugated laminates for morphing applications is given by Airoldi et al. [24]. Previtali et al. [25] considered a particular corrugated-shape design with enhanced bending stiffness about the span direction for morphing wings. Takahasi et al. [26] et al. developed a variable-camber wing with morphing leading and trailing sections using corrugated structures. Bai et al. [27] suggest a flexible-skin design for morphing applications where two corrugated laminates are bonded together so that a symmetric structure results. Henry et al. [28] and Gong et al. [29] consider a morphing-wing concept with distributed piezoelectric actuation and a corrugated flexible-skin section.
Thurnherr et al. [30] investigated the static response to homogeneous pressure of highly anisotropic corrugated sheets. Ermakova and Dayyani [31] performed shape optimization of composite corrugated morphing skins to improve resistance against aerodynamic loads.
Shaw et al. [32] optimized corrugated laminates for buckling in morphing aircraft.
Thill et al. [33] and Xia et al. [34] studied experimentally and computationally the effect of a corrugated skin on the global aerodynamics of an airfoil. Dayyani et al [35] suggested and investigated a wing design with skins made from trapezoidal cores coated with elastomeric skins. Dayyani and Friswell [36] considered static as well as aerodynamic aspects within their multi-objective optimization for the geometry of trapezoidal corrugated morphing skins. Filipovic and Kress [16] suggested a corrugation design and manufacturing method for corrugated laminates with a circular-sections corrugation shape and added scales for an aerodynamically smooth surface.

1.2.2 Structural load-carrying behavior

With hind-side to applications as flexible skins in morphing-wing design, Thurnherr et al. [30] studied the structural response of high-amplitude corrugated laminates to pressure.

1.2.3 Energy absorbing potential

The corrugations transform in-plane elongation transverse to the corrugation into local bending which creates interlaminar stress and provokes delamination failure with high energy-absorption potential. The phenomenon was also observed in the experimental part of the work by Soltani et al. [11]. Ren et al. [37–39] have contributed to damage progression modeling to predict crashworthiness of corrugated laminates and strut structures.

1.2.4 Sandwich corrugated core design

Buannic et al. [40] developed a homogenization model of corrugated core sandwich panels. Aboura et al. [41] performed an experimental and analytical study on the elastic behavior of cardboard. Biancolini [42] evaluated equivalent stiffness properties of corrugated board. Talbi et al. [43] developed an analytical homogenization model for finite-element modeling of corrugated cardboard. Kazemahvazi and Zenkert [44] modeled corrugated all-composite sandwich structures and Kazemahvazi et al. [45] performed experiments to study failure mechanisms in such structures. Abbès and Guo [46] found an analytic homogenization model for torsion of orthotropic sandwich plates. Dayyani et al. [47] developed equivalent models of composite corrugated cores with elastomeric coatings for morphing aircraft. Bartolozzi et al. [48, 49] invented a general analytical method for finding the equivalent properties for corrugated cores of sandwich structures. Cheon and Kim [50] contributed an equivalent model for corrugated sandwich panels. Isaksson and Carlson [51] analyzed the out-of-plane compression and shear response of paper-based web-core sandwiches.

1.3 Homogenized substitute-plate models

Homogenized substitute-plate, or equivalent models, describe the global structural response of periodically corrugated structures. Such models eliminate the need for detailed numerical mapping of the corrugated geometry of large structures with many corrugations and enable thus numerically efficient simulations and structural optimization processes. The equivalent models take advantage of both, the periodicity and the assumption of large extension transverse to the corrugations. In 1986, Briassoulis [52] derived equivalent orthotropic properties of a corrugated sheet. Shimansky and Lele [53] considered the stiffness transverse to the corrugations of a sinusoidally corrugated metal sheet. Later, Yokozeki et al. [54] calculated such properties for corrugated strictly orthotropic laminates. Kress and Winkler [55] worked out exact thin-shell-theory solutions for corrugated symmetric cross-ply laminates, where the corrugation shape consists of circular segments. The same authors considered in-plane extension and in-plane shear as well as bending and twist macro deformations to find the entries of a substitute ABD matrix. Xia and Friswell [56] invented a concept that can calculate the substitute stiffnesses for any corrugation shape. Xia et al. made further contributions in [57]. Mohammadi et al. [58] developed an equivalent model for trapezoidal cor-

rugation shapes. Wang et al. [59] consider laminates with axial and bending coupling. Nguyen-Minh et al. [60] use existing homogenization models in their analysis. Moro et al. [61] reviewed the model by Kress and Winkler [55] and extended it for more general laminate designs. However, thin-shell theory cannot account for the through-thickness effects that have an influence on the behavior of corrugated laminates. This problem was circumvented by Kress and Winkler [62] by inventing a planar finite-element formulation that maps only the cross-section of one periodic cell of the corrugated laminates. This model takes into account all mechanical effects and is not restricted to thin laminates; it can calculate three-dimensional stress states accurately and produces a substitute-plate ABD matrix for arbitrary laminates at low numerical cost. Park et al. [63] evaluated homogenized effective properties for corrugated composite panels. Aoki and Maysenhölder [64] provide a critical review on existing substitute-plate models.
The same assumptions that enable all of the efficient substitute-plate or equivalent-plate models to exist, namely very long extension along both in-plane directions, restrict the solution space to the inner solution.

1.4 Free-edge effects

Research on free-edge effects has played a prominent role for better understanding the mechanics of composite materials. It is helpful to imagine tensile tests on rectangular laminate coupons: the elastic coupling effects of the layers made from anisotropic materials constrain each other in the laminate so that stresses appear not only in the loading direction but also in the inplane transverse direction. The latter stress components must vanish at the free edges which necessarily leads to stress gradients. Consequently, local equilibrium gives rise to interlaminar stresses and cross-sectional warping.
Pioneering work on free-edge effects has been done by Pipes and Pagano [65] and Hsu and Herakovich [66]. The interlaminar stresses can lead to edge delamination the progress of it can be predicted by fracture-mechanics concepts. O'Brien [67] invented a quite simple model for calculating the total strain energy rate from a global energy balance to be evaluated by means of the classical theory of laminated plates. Analytical solutions stem from Wang and Choi [68] and Whitcomb and Raju [69]. Kress developed a planar finite-element formulation to be able to study the edge effects in arbitrary laminate designs and their effects on measured-stiffness [70] and measured-strength [71] predictions. Becker found closed-form solutions for free-edge effects in cross-ply laminates [72] and Becker and Kress [73] considered the stiffness reduction in laminate coupons due to the free-edge effect. More recent research is due to Mittelstedt and Becker [74], Dhanesh et al. [75], and Hajikazemi and Paepegem [76].
We mention this research on flat laminates as an introductory analogy because we did not find a systematic study on free-edge effects of corrugated laminates. The only work reflecting influence of support conditions and aspect ratio on corrugated sheet metal known to us is the comprehensive analytical and experimental study on the stability of anisotropic plates performed by Seydel [77].

1.5 Contents and structure of the present work

The objective of this work is to illuminate the influence of boundary conditions on structural stiffness of corrugated laminates with circular-sections corrugation shape. Analog to our work on substitute-plate models [55, 62] we distinguish six different load cases corresponding to the line loads considered in the classical theory of laminated plates. We perform structural analysis with FEM on rectangular corrugated sheets where two opposite edges are clamped and the other two edges are free. The parameters include the distance between the supports and the corrugation amplitude. We present structural stiffness values normalized with respect to the respective substitute-plate properties found with [62].

2 FEM modeling

In the following examples, corrugated laminates where the reference configuration is a periodic corrugation pattern consisting of circular sections are considered. The laminates are much thinner than the circular-sections radii, which enables the comparison of the simulation results to homogenization models which are based on thin-shell theory.

2.1 Unit cell geometry

The geometry of a corrugation pattern consisting of circular sections is shown in Figure 1. Center-line points are described with

$$\begin{aligned} y^{(0)}(\xi_2) &= R sin\Delta\psi \\ z^{(0)}(\xi_2) &= R\,[1 - cos\Delta\psi] - c, \end{aligned} \tag{1}$$

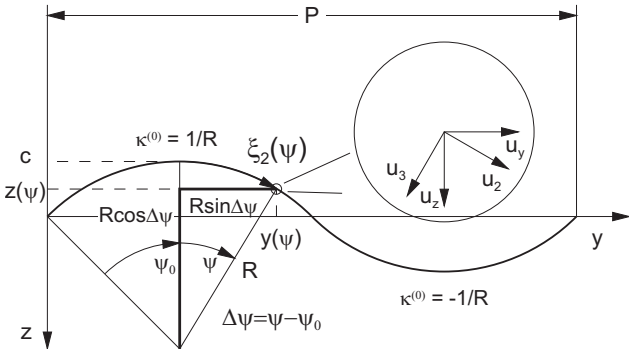

Figure 1: Unit-cell geometry and coordinate conventions

where

$$\Delta\psi = \psi - \psi_0 = \frac{\xi_2}{R} - \psi_0 = \kappa^0 \xi_2 - \psi_0 \,, \tag{2}$$

where the angle ψ_0 is a shape characteristic depending on the normalized corrugation amplitude c/P:

$$\psi_0 = acos\left(1 - \frac{c}{R}\right) \,. \tag{3}$$

Specified periodic length P and corrugation amplitude c determine the mid-plane curvature radius R:

$$R = \frac{16c^2 + P^2}{32c} \tag{4}$$

where the condition that the reference configuration must not penetrate itself limits c to

$$0 \le c \le \frac{P - t + \sqrt{(P-t)^2 - \frac{P^2}{4}}}{2} \,, \tag{5}$$

where t is laminate thickness.

2.2 Simulation setup

The finite element simulations were carried out using the commercial software ANSYS ©, version 19.2 [78]. The APDL input files, which contain all the relevant data on nodal points, meshing, elements and boundary conditions, were generated in a MATLAB © [79] routine and then transmitted to the FE program using the batch mode.

In order to be able to accurately map the occurring effects, the Solid186 element, which contains 20 nodes and quadratic shape functions, was used. The drawback is that the chosen element is quite costly, leading to a high computational effort for large simulations. This problem was mitigated by using a mesh data base in MATLAB ©, where nodal-point positions were stored for the selected configurations, allowing to refrain from recalculating them for every simulation. Furthermore the number of cores in ANSYS © was increased in order to speed up the simulations.

In the given study, only linear simulations were performed, which ensures comparability to existing homogenization models. Hence, the resulting stiffness values can be considered initial values, which reflect reality at the beginning of the deformation.

2.3 Boundary conditions

Homogenization models simulate interior solutions that appear in large and homogeneously loaded corrugated sheets far away from their edges. Interior solutions are marked by periodicity of state variables that is simulated by applying a combination of boundary conditions and periodicity conditions to a unit cell.
The present study investigates complete solutions where interior solutions are perturbed with clamping as well as free-edge effects. The essential boundary conditions are chosen to simulate the effects of realistic clamps: All degrees of freedom along a clamped edge are prescribed. Clamped edges are indicated in Figures 3 through 8 with dark shaded areas.

2.3.1 Load cases

The load information is specific for each of the thin-plate load cases shown in Figure 2 used for establishing homogenized substitute-plate models [55, 62, 63]. For the individual load cases addressed in the following paragraphs, the inhomogeneous essential boundary conditions will be explicitly stated and it will be implied that all other degrees-of-freedom at the same boundary underly homogeneous essential boundary conditions.

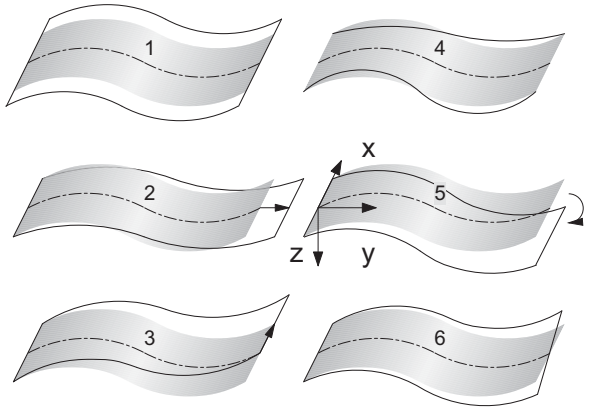

Figure 2: Load cases illustration (after [55])

In the following explications, L_x corresponds to the length of the corrugated laminate transverse to the corrugations, P to the unit cell width (as defined in Chapter 2.1) and n to the number of cells modeled in the simulation.

2.3.1.1 Load case 1

For this load case the edges at $x = \pm L_x/2$ are clamped with the rigid clamps being moved apart as Figure 3 indicates.

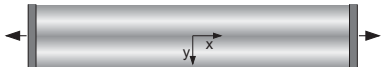

Figure 3: Load case 1 illustration (for $n = 1$).

This situation is simulated with the specified displacements:

$$\begin{aligned} x = -\frac{L_x}{2}: \quad \hat{u}_x = 0: \qquad & \hat{u}_y = \hat{u}_z = 0 \\ x = \quad \frac{L_x}{2}: \quad \hat{u}_x = L_x\varepsilon^0_{xx}: \quad & \hat{u}_y = \hat{u}_z = 0 \end{aligned} \tag{6}$$

2.3.1.2 Load case 2

For this load case the edges at $y = \pm nP/2$ are clamped whereas the rigid clamps are moved apart as Figure 4 indicates. Modeling only one unit cell ($n = 1$) is expected to give an upper bound for the influence of edge clamping.

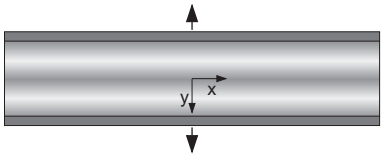

Figure 4: Load case 2 illustration

The situation can be simulated by specifying the following displacements along the clamps:

$$\begin{aligned} y = -\frac{nP}{2}: \quad \hat{u}_y = 0: \qquad & \hat{u}_x = \hat{u}_z = 0 \\ y = \quad \frac{nP}{2}: \quad \hat{u}_y = P_n\varepsilon^0_{yy}: \quad & \hat{u}_x = \hat{u}_z = 0 \end{aligned} \tag{7}$$

2.3.1.3 Load case 3

For this load case we propose that the rigid clamps at edges $y = \pm nP/2$ are moved along x in opposite directions as Figure 5 indicates. Increasing the aspect ratio $L_x/(n \cdot P)$ will lead to a higher influence of clamping, while a reduction of the same parameter is expected to facilitate free-edge effects.

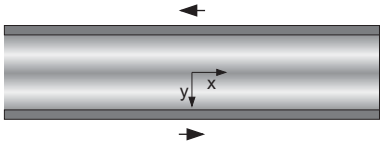

Figure 5: Load case 3 illustration

The situation can be simulated by applying the following essential boundary conditions, specified at the clamps:

$$\begin{aligned} y = -\frac{nP}{2}: \quad \hat{u}_y = 0: \qquad & \hat{u}_x = \hat{u}_z = 0 \\ y = \quad \frac{nP}{2}: \quad \hat{u}_y = P_n\varepsilon^0_{yy}: \quad & \hat{u}_x = \hat{u}_z = 0 \end{aligned} \tag{8}$$

2.3.1.4 Load case 4

For this load case we propose that the edges at $x = \pm L_x/2$ are clamped and that the rigid clamps are rotated by $\varphi_y = \frac{L_x}{2}\varepsilon^1_{yy}$ as Figure 6 indicates.

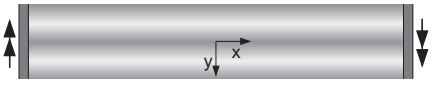

Figure 6: Load case 4 illustration

This situation is simulated by specifying the following essential boundary conditions at the clamps:

$$\begin{aligned} & x = -\frac{L_x}{2}: \\ & u_x = -\frac{L_x}{2} z\varepsilon^1_{yy} \quad u_y = 0 \quad u_z = -\frac{1}{2}\left(\frac{L_x}{2}\right)^2\varepsilon^1_{yy} \\ & x = \quad \frac{L_x}{2}: \\ & u_x = \quad \frac{L_x}{2} z\varepsilon^1_{yy} \quad u_y = 0 \quad u_z = -\frac{1}{2}\left(\frac{L_x}{2}\right)^2\varepsilon^1_{yy} \end{aligned} \tag{9}$$

2.3.1.5 Load case 5

For this load case we propose that the rigid clamps at edges $y = \pm nP/2$ are rotated about x in opposite directions as

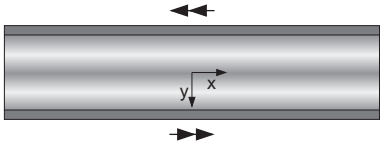

Figure 7: Load case 5 illustration

Figure 7 indicates. This situation is simulated by applying the rotation $\varphi_x = \frac{nP}{2}\hat{\kappa}_y$ along x at the clamps:

$$
\begin{aligned}
&y = -\frac{nP}{2}: \\
&u_x = 0 \qquad u_y = -cos(\phi)\varphi_x z_3 \quad u_z = sin(\phi)\varphi_x z_3 \\
&y = \frac{nP}{2}: \\
&u_x = 0 \qquad u_y = cos(\phi)\varphi_x z_3 \quad u_z = -sin(\phi)\varphi_x z_3
\end{aligned}
\tag{10}
$$

where the angle ϕ describes the inclination of the edges with respect to the z-axis and z_3 the distance to the laminate mid-plane.

2.3.1.6 Load case 6

For this load case we propose that the rigid clamps at the edges $y = \pm nP/2$ are rotated about the y-axis as Figure 8 indicates

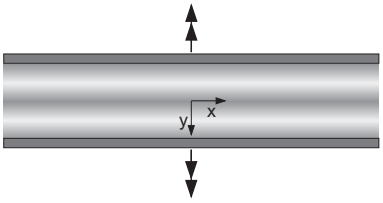

Figure 8: Load case 6 illustration

This situation is simulated with the following essential boundary conditions applied at the edges:

$$
\begin{aligned}
&y = -\frac{nP}{2}: \\
&u_x = \frac{1}{2}yz\varepsilon^1_{xy} \quad u_y = \frac{1}{2}xz\varepsilon^1_{xy} \quad \hat{u}_z = -\frac{1}{2}xy\varepsilon^1_{xy} \\
&y = \frac{nP}{2}: \\
&u_x = \frac{1}{2}yz\varepsilon^1_{xy} \quad u_y = \frac{1}{2}xz\varepsilon^1_{xy} \quad \hat{u}_z = -\frac{1}{2}xy\varepsilon^1_{xy}
\end{aligned}
\tag{11}
$$

2.4 Structural stiffness evaluations

As the loading is applied in terms of specified strain or curvature, which may be translated to specified displacements or rotations, the calculation of structural stiffness requires the evaluation of nodal reactions to form line loads or line moments.

The fully constrained versions of the six load cases are expected to reconstruct the substitute-plate $\tilde{A}\tilde{B}\tilde{D}$ matrix that can also be calculated with homogenized-substitute-plate models, in the limiting case of a flat laminate this would be the laminated-plate ABD matrix. As the fully constrained cases thus give opportunity for model verification, the less constrained cases map free-edge effects, thereby providing information on the applicability limits of existing inner solutions.

Depending on the load case, the line loads need to be evaluated either along the line $x = -L_x/2$ or along $y = -nP/2$. In the first case, the average line loads can be calculated from the nodal reactions as follows:

$$
\begin{aligned}
N_x &= -\frac{1}{nP}\sum_{k=1}^{N_{nx}} f_{x_k} \\
N_{xy} &= -\frac{1}{nP}\sum_{k=1}^{N_{nx}} f_{y_k} \\
M_x &= -\frac{1}{nP}\sum_{k=1}^{N_{nx}} f_{x_k} z_k \\
M_{xy} &= -\frac{1}{nP}\sum_{k=1}^{N_{nx}} (f_{z_k} y_k - f_{y_k} z_k)
\end{aligned}
\tag{12}
$$

where f_i are the nodal forces and N_n the number of evaluated nodes.

Similarly, the reactions along the line $y = -nP/2$ are evaluated as follows:

$$
\begin{aligned}
N_y &= -\frac{1}{L_x}\sum_{k=1}^{N_{nx}} f_{y_k} \\
N_{yx} &= -\frac{1}{L_x}\sum_{k=1}^{N_{nx}} f_{x_k} \\
M_y &= -\frac{1}{L_x}\sum_{k=1}^{N_{nx}} (f_{y_k} z_k + f_{z_k} y_k) \\
M_{yx} &= -\frac{1}{L_x}\sum_{k=1}^{N_{nx}} (f_{z_k} x_k - f_{x_k} z_k)
\end{aligned}
\tag{13}
$$

The measured stiffness reflects resistance against a combination of uniaxial stress and clamping effects. For conciseness, the geometry parameters $L^\star$ and $t^\star$, normalized with respect to periodic length P, $L^\star = L_x/(nP)$ and $t^\star = t/(nP)$, are introduced.

2.4.1 Load case 1 stiffness measurement

The stiffness measurement of load case 1, C^0_x, is obtained with the line force N_x in (12):

$$
C^0_x = \frac{N_x}{\varepsilon_x} \tag{14}
$$

For large $L^\star$, load case 1 obtains, for a homogeneous material, it's Young's modulus E, and for a flat or corrugated

laminated an apparent averaged Young's modulus. For small $L^\star$, load case 1 approximately obtains, for a flat laminate, the stiffness A_{11} and a higher value than that for a corrugated laminate, respectively, as the displacement field is constrained at the clamps.

2.4.2 Load case 2 stiffness measurement

The stiffness measurement of load case 2, C_y^0, is obtained with the line force N_y in (13):

$$C_y^0 = \frac{N_y}{\varepsilon_y} \tag{15}$$

For small $L^\star$, load case 2 obtains, for a homogeneous material, it's Young's modulus E, and for a flat or corrugated laminate an apparent averaged Young's modulus. With increasing length $L^\star$, C_y^0 increases asymptotically to A_{22}.

2.4.3 Load case 3 stiffness measurement

The stiffness measurement of load case 3, C_{xy}^0, is obtained with the line force N_{xy} in (13):

$$C_{xy}^0 = \frac{N_{xy}}{\gamma_{xy}} \tag{16}$$

For large $L^\star$, load case 3 obtains for a flat or corrugated symmetric and balanced laminate the apparent averaged shear stiffness $\tilde{A}_{66}$. With decreasing aspect ratio $L^\star$, C_{xy}^0 tends to zero.

2.4.4 Load case 4 stiffness measurement

The stiffness measurement of load case 4, C_{xx}^1, is obtained with the line moment M_{xx} in (12):

$$C_{xx}^1 = \frac{M_x}{\kappa_{xx}} \tag{17}$$

For large $L^\star$, load case 4 obtains for a flat or corrugated symmetric laminate the apparent bending stiffness,

$$C_{xx}^1 \approx D_{11} + \frac{2D_{12}D_{16}D_{26} - D_{22}D_{16}^2 - D_{66}D_{12}^2}{D_{22}D_{66} - D_{26}^2}\,. \tag{18}$$

For small $L^\star$, load case 4 obtains in case of corrugated laminates values higher than D_{11} because of the clamping constraint of $u_y = u_z = 0$.

2.4.5 Load case 5 stiffness measurement

The stiffness measurement of load case 5, C_{yy}^1, is obtained with the line moment M_y in (13):

$$C_{yy}^1 = \frac{M_y}{\kappa_{yy}} \tag{19}$$

For small $L^\star$, load case 5 obtains for a flat or corrugated symmetric laminate the apparent bending stiffness,

$$C_{yy}^1 \approx D_{22} + \frac{2D_{12}D_{16}D_{26} - D_{11}D_{26}^2 - D_{66}D_{12}^2}{D_{11}D_{66} - D_{16}^2}\,. \tag{20}$$

2.4.6 Load case 6 stiffness measurement

The stiffness measurement of load case 6, C_{yx}^1, is obtained with the line moment M_{yx} in (13):

$$C_{yx}^1 = \frac{M_{yx}}{\kappa_{yx}} \tag{21}$$

For large dimensions, load case 6 is expected to approach the apparent averaged twist stiffness $\tilde{D}_{66}$ for a flat or corrugated symmetric and balanced laminate.

3 Parameter Study

The structural analysis considers materials and laminates as well as corrugation amplitudes c, where the flat plate $c = 0$ allows verification with the results of the classical theory of laminated plates.

3.1 Materials

We consider a homogeneous corrugated sheet made from aluminum as well as several laminates made from the highly anisotropic carbon-fiber reinforced plastic (CFRP) with GY70 carbon fibers. The properties of aluminum are given with $E = 70000\,MPa$ and $\nu = 0.3$ whereas those of the unidirectional and transverse isotropic CFRP composite are given in Table 1, where the subscript 1 indicates fiber direction and subscripts 2 and 3 the directions transverse to the fibers.

Table 1: Relevant material properties of unidirectional GY70/epoxy with fiber-volume fraction $v_f = 0.6$ (moduli in MPa). Source: DORNIER SYSTEM GmbH

E_1	E_2, E_2	ν_{23}	ν_{13}, ν_{12}	G_{23}	G_{13}, G_{12}
290000	5000	0.2	0.41	2083	5000

3.2 Laminates

The isotropic and homogeneous aluminum sheet of thickness $t = 1\,mm$ serves as a reference for the various anisotropic CFRP laminates that explore the materials design space. The selected lay-ups were chosen due to their differing properties:

1. $[0_4]$ high extensional stiffness transverse to the corrugated direction
2. $[90_4]$ high extensional stiffness along the corrugated direction
3. $[\pm 45]_s$ high shear, low extensional stiffness

Each laminate consists of four layers having a thickness $h = 0.25\,mm$ so that all sheets or laminates have a total thickness of $t = 1\,mm$.

3.2.1 ABD matrix homogeneous sheets and laminates

Isotropic materials or unidirectional laminates couple strain in one direction with line force along the other respective direction and bending about one direction with a bending line moment about the other respective direction. These couplings are due to Poisson's ratio.

$$\begin{matrix} A_{11} & A_{12} & 0 & 0 & 0 & 0 \\ A_{12} & A_{22} & 0 & 0 & 0 & 0 \\ 0 & 0 & A_{66} & 0 & 0 & 0 \\ 0 & 0 & 0 & D_{11} & D_{12} & 0 \\ 0 & 0 & 0 & D_{12} & D_{22} & 0 \\ 0 & 0 & 0 & 0 & 0 & D_{66} \end{matrix} \tag{22}$$

3.2.2 ABD matrix symmetric angle-ply laminate

Symmetric angle-ply laminates are balanced but exhibit an additional coupling between bending curvature and torque or twist and bending moment, respectively.

$$\begin{matrix} A_{11} & A_{12} & 0 & 0 & 0 & 0 \\ A_{12} & A_{22} & 0 & 0 & 0 & 0 \\ 0 & 0 & A_{66} & 0 & 0 & 0 \\ 0 & 0 & 0 & D_{11} & D_{12} & D_{16} \\ 0 & 0 & 0 & D_{12} & D_{22} & D_{26} \\ 0 & 0 & 0 & D_{16} & D_{26} & D_{66} \end{matrix} \tag{23}$$

3.2.3 Resistances against sheet laminate deformations

Table 2 compares plate-stiffness matrix entries with the apparent stiffness values reflecting lack of deformation constraint. Figure 9 gives a visual impression of the relative differences between constrained and unconstrained stiffness values. It appears that those differences are extremely small for the unidirectional composites and rather large for the laminate $[\pm 45]_s$. It is only for the latter laminate that the torsional stiffnesses are different from each other which is due to the fully coupled bending stiffness matrix **D** indicated in (23). The constrained and unconstrained

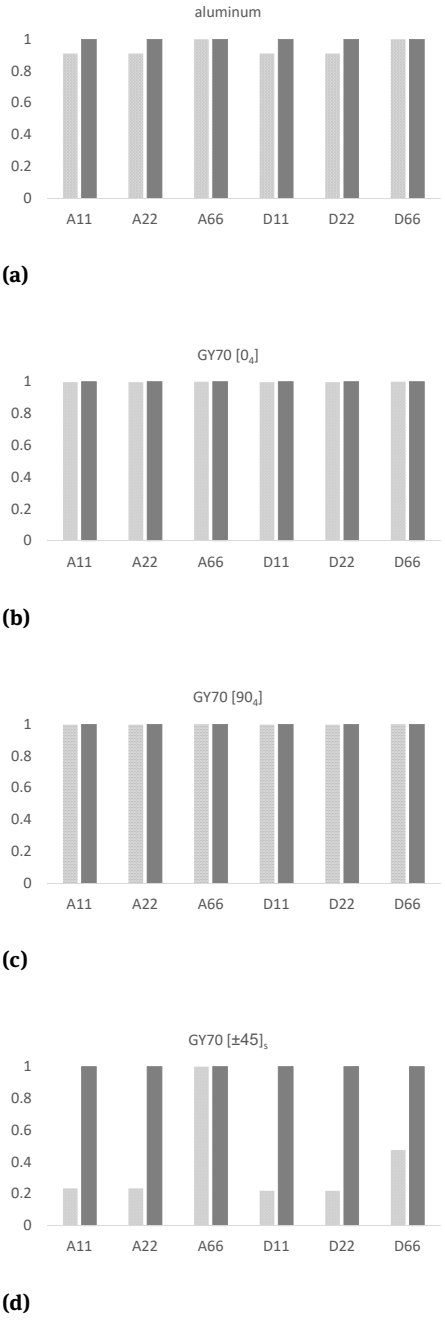

Figure 9: Constrained (darker gray) versus unconstrained (lighter gray) stiffness values

Table 2: Resistances against constrained and unconstrained deformation

C	Alu	$[0_4]$	$[90_4]$	$[\pm 45]_s$
A_{11}	76923.1	290843.	5014.53	79992.3
A^u_{11}	70000.0	290000.	5000.00	18749.9
A_{22}	76923.1	5014.53	290843.	79992.3
A^u_{22}	70000.0	5000.00	290000.	18749.9
D_{11}	6410.26	24236.9	417.878	6666.03
D^u_{11}	5833.34	24166.7	416.667	1461.47
D_{22}	6410.26	417.878	24236.9	6666.03
D^u_{22}	5833.34	416.667	24166.7	1461.47
D_{66}	2243.58	416.667	416.667	6078.03
D^u_{66}	2243.58	416.667	416.667	2886.38

membrane shear stiffness values are always the same because all laminates are balanced.

3.3 Geometries

The unit cell-length is fixed at $P = 100\,mm$ and the thickness is always $t = 1\,mm$. The corrugation shape is always composed of circular segments as is detailed in Section 2.1.

Corrugation amplitudes include with $c = 0\,mm$ a flat plate, with $c = 5\,mm$ a mildly corrugated sheet, and with $c = 25\,mm$ a highly corrugated sheet. This corrugation amplitude corresponds with semi-circles and marks the limit of what can be manufactured with the help of molds.

The non-dimensional geometry parameters, where the periodic length is used for normalization, are $t^\star = 0.01$ and $c^\star = 0, 0.05, 0.25$.

4 Inner solution reference values verification

The present paper gives us the opportunity to correct a mistake that went unnoticed when we published our closed-form shell-theory model for corrugated laminates [55]: the result stated in there, namely that the torsional stiffness is invariant with respect to corrugation amplitude c, $\tilde{D}_{66} = D_{66}$, is wrong. The correct solution, which we had found earlier and was placed in [80], is given with

$$\tilde{D}_{66} = \frac{\psi_0}{S^{(1)}} D_{66}\,, \quad S^{(n)} = sin\,(n\psi_0)\,,\ n = 1 \qquad (24)$$

where the the opening angle ψ_0 of the circular-sections corrugation shape is defined in Figure 1.

We use classical laminated plate theory (CLPT) to calculate the flat ($c = 0$) plate stiffness values seen in Table A1 in A. For calculating the homogenized-plate substitute values of corrugated laminates with corrugation amplitudes $c = 5\,mm$ and $c = 25\,mm$ we use our closed-form model (CF) after the theory in [55] with the correct result in (24) and our planar finite-element model (FE) where the theory is explained in [62], with the adaption that the line moment used for calculating the torsional stiffness $\tilde{D}_{66}$ is calculated as follows:

$$M_{xy} = \frac{1}{P} \int_\Omega (\tau_{xy} z - \tau_{xz} y)\, d\Omega. \qquad (25)$$

It can be seen that the agreement between the predictions of the two different models is excellent for most value pairs. The maximum deviation between the two solutions is 2.2%, except for the case of the torsional stiffness $\tilde{D}_{66}$, where the agreement is good for the case of the plate and then deteriorates for larger corrugation amplitudes. These larger deviations are traced back to the influence of through-thickness effects that are correctly mapped with the planar finite-element model and that elude the thin-plate closed-form model. The problem is discussed in more detail below, where the different results are explained using the example of the circularly corrugated laminate.

As Table A1 shows, there seems to be a large offset between the analytical shell-theory model and the finite element routine when it comes to determining the substitute plate value $\tilde{D}_{66}$ for corrugated laminates. For the case of the semi-circular corrugated laminate the two solutions differ more or less by factor two, independently of the selected lay up. For smaller values of amplitude, the difference is less pronounced and vanishes for flat plates. This deviation can be explained by studying the evaluation mechanisms in both cases - in the "shell world" as well as the "solid world".

The resulting stress distribution in a homogeneous corrugated laminate subjected to torsional loading is qualitatively shown in Figure 10 for the case of the semi-circular corrugation. The shear stresses are linearly distributed over the thickness, hence, they vanish at the laminate mid-

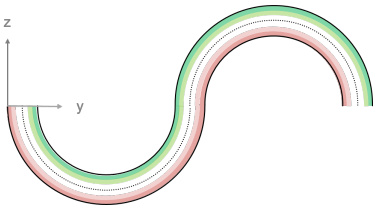

Figure 10: Stress distribution in a corrugated laminate of "infinite width" subjected to torsional loading.

plane. Since infinite width of the laminate is assumed, there are no edge effects visible at the ends of the unit cell.

In Figure 11 all the parameters relevant in shell theory are shown. The linear distribution of the shear stresses over the laminate thickness d can be represented in the local s, t-coordinate-system:

$$\tau_{shell}(t) = 2 \cdot \tau_{max} \cdot \frac{t}{d} \tag{26}$$

The equation above respects the boundary condition that the shear stress is maximum at the surfaces of the laminate. In shell models, a local moment with respect to the laminate mid-plane is then usually calculated:

$$M_{loc}^{(x)} = -\int_{-\frac{d}{2}}^{\frac{d}{2}} \tau_{shell}(t) \cdot t \, dt \tag{27}$$

where the moment is defined positively about the x-axis. The total moment about the x-axis in the arc can then be found by multiplication with the respective arc length:

$$M_{shell}^{(x)} = \pi R \cdot M_{loc}^{(x)} = -\frac{1}{6} \cdot \pi R \cdot \tau_{max} \cdot d^2 \tag{28}$$

where R refers to the distance to the laminate mid-plane.

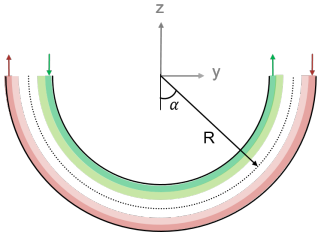

Figure 11: Stress distribution in a corrugated laminate half-cell subjected to torsional loading. The plot shows the relevant parameters known in shell theory models.

Now, the situation when using the planar finite element model is investigated, which can be represented using cylindrical coordinates as defined in Figure 12. As before, the shear stresses are assumed to be linearly distributed over the laminate thickness:

$$\tau_{cyl}(r) = -2 \cdot \tau_{max} \cdot \frac{r}{d} + 2 \cdot \tau_{max} \cdot \frac{R}{d} \tag{29}$$

The total moment about the x-axis can then be directly integrated using cylindrical coordinates:

$$M_{cyl}^{(x)} = \int_{R-\frac{d}{2}}^{R+\frac{d}{2}} \int_{-\frac{\pi}{2}}^{\frac{\pi}{2}} \tau_{cyl}(r) \cdot r \, r \, d\alpha \, dr \tag{30}$$

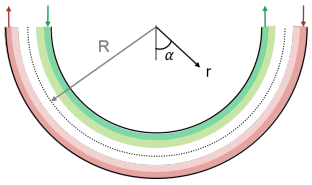

Figure 12: Stress distribution in a corrugated laminate half-cell subjected to torsional loading. The plot shows the relevant parameters known in planar models.

Evaluation of equation (30) yields:

$$M_{cyl}^{(x)} = -\frac{1}{3} \cdot \pi R \cdot \tau_{max} \cdot d^2 \tag{31}$$

Comparison of the values obtained in equations (28) and (31) shows that the two different evaluation approaches will produce resulting moments which differ by a factor 2, although the assumption for the shear stress distribution is identical in both cases. As a consequence, the calculated torsional stiffness will also show the same dependency. Note that this deviation can also be observed if the results of finite element simulations conducted using shell elements are compared to results of corresponding simulations with solid elements.

The results obtained using the shell models can be reproduced in cylindrical cooordinates by adapting the differential of the arc length in a way that the coordinate r is replaced by the distance to the mid plane R:

$$\int_{R-\frac{d}{2}}^{R+\frac{d}{2}} \int_{-\frac{\pi}{2}}^{\frac{\pi}{2}} \tau_{cyl}(r) \cdot r \, \mathbf{R} d\alpha \, dr = M_{shell}^{(x)} \tag{32}$$

Hence, one can conclude that in shell models the behavior in radial direction is not sufficiently reproduced since the mid-plane is always taken as the reference. In combination with the peculiar geometry of the round corrugations, this leads to a quite large deviation in the prediction of the substitute torsional stiffness $\tilde{D}_{66}$.

4.1 Given Study

The model for analyzing edge effects uses finite solid elements that also map through-thickness effects. This model asymptotically approaches the inner solution for extreme plate-geometry aspect ratios. Consistently, the agreement is better with the FEM homogenization model than with the closed-form solution. Therefore, the FEM homogenization model predictions of the inner solution (bold text in Table A1 in A) are used as a reference for all load cases, laminate designs, and corrugation amplitudes.

5 Validity ranges of substitute-plate stiffness values

We investigate the influence of length L_x transverse to the corrugations and - if necessary - the number of unit cells on overall stiffness. Each of the diagrams in Figures 13 through 22 contains the stiffness developments for flat ($c = 0$), low-amplitude ($c = 5mm$), and moderately-high-amplitude ($c = 25mm$) corrugation shapes. All curves are normalized with respect to the interior-solution stiffness values obtained by our homogenization model [62], so that results verification can be obtained from the diagrams. The respective load case are addressed in the following sections where each section considers the influence of the sheet material.

5.1 Load case 1: strain in out-of-plane direction

Load case 1 applies strain transverse to the direction of the corrugations. For this load case the plate width P remains constant (width of one unit cell) whereas the distance between the clamps L_x changes. The corresponding stiffness maps can be found in Figure 13.

As the clamps prevent deformation within the $y - z$ plane, small clamp distances create loading situations similar to the assumptions of homogenization models. For this reason the apparent stiffnesses of the flat sheets of all materials agree with the inner solution at small distances L_x between the clamps. At large distances between the clamps the loading situation is dominated by uniaxial stress so that the apparent stiffness values approach those of the respective (averaged) Young's moduli. The differences between plate stiffness and the respective Young's moduli are particularly small for the unidirectional composites and quite large for the angle-ply laminate, as seen in the corresponding diagrams in Figure 13.

In contrast to that, the apparent stiffnesses of the corrugated sheets approach the inner-solution values at large distances between the clamps and are higher than that at short distances. This behavior is attributed on the one hand to the fact that the clamps prevent corrugation-shape changes and on the other hand to the fact that the high compliance of corrugated sheets along the directions of the corrugations minimizes the effect of displacement constraint along the latter direction.

For practical purposes, it can be noted that the apparent stiffness of the unidirectional materials is very close

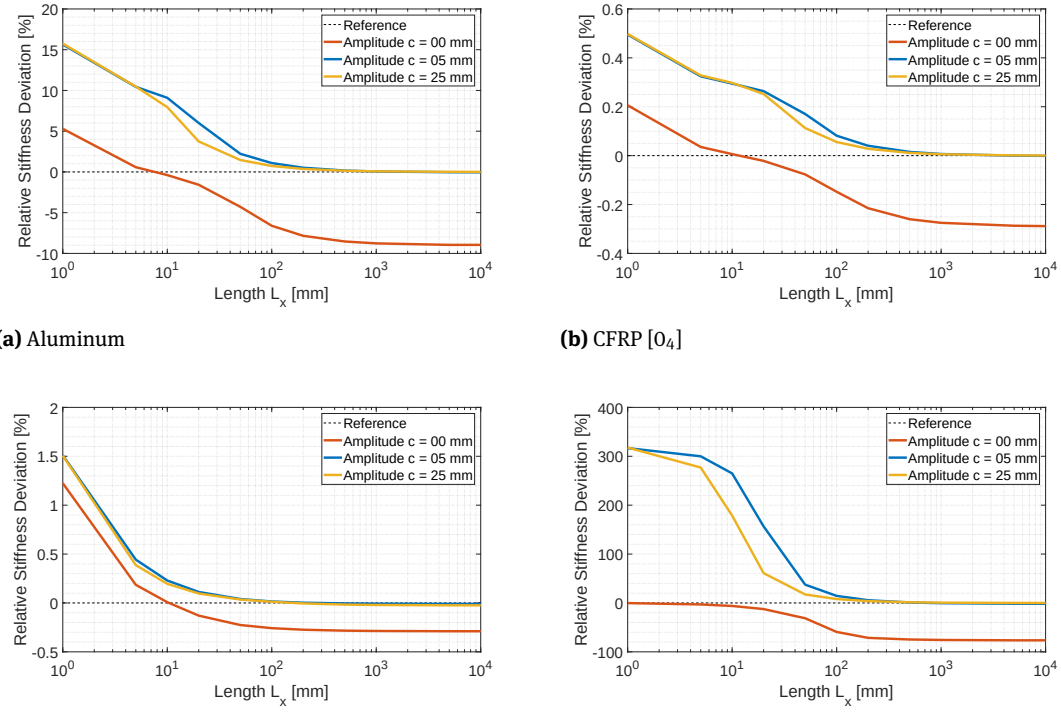

(a) Aluminum

(b) CFRP $[0_4]$

(c) CFRP $[90_4]$

(d) CFRP $[\pm 45]_s$

Figure 13: Load case 1 normalized apparent stiffnesses versus L_x for constant width P (one unit cell).

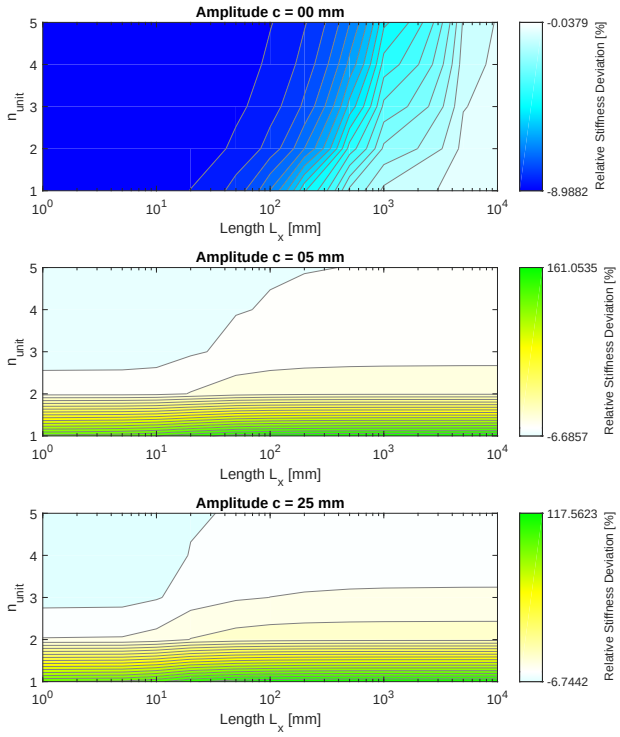

(a) Aluminum

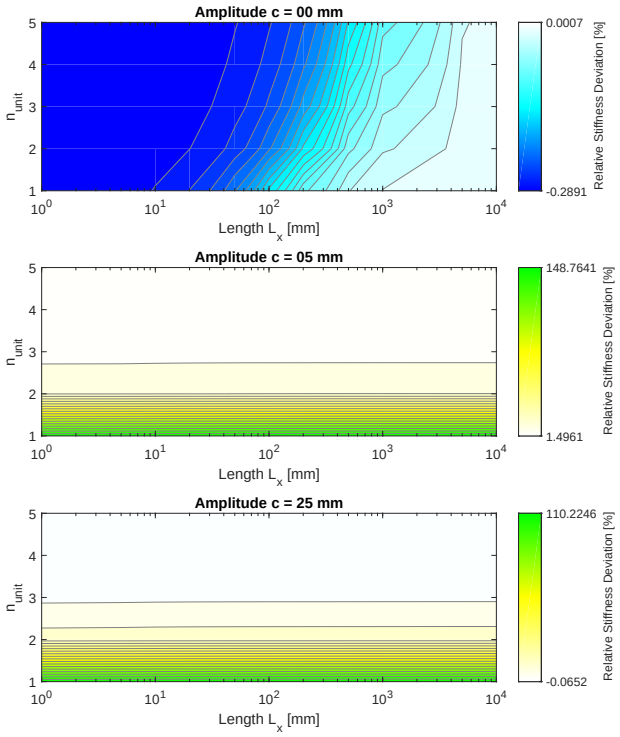

(c) CFRP $[90_4]$

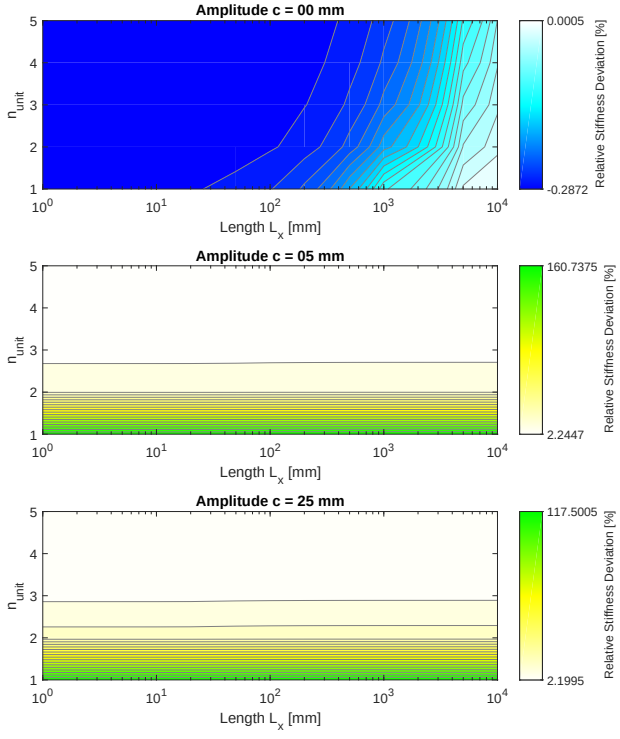

(b) CFRP $[0_4]$

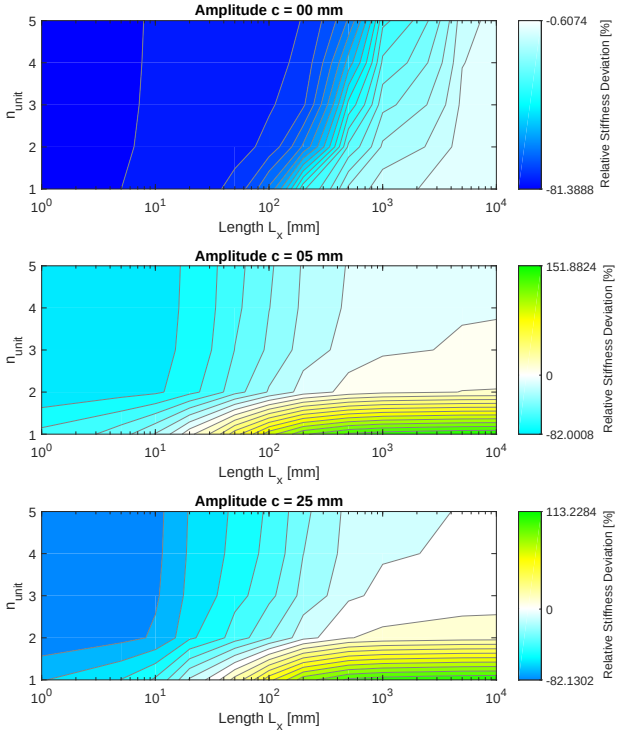

(d) CFRP $[\pm 45]_s$

Figure 14: Load case 2 normalized apparent stiffnesses versus L_x and n_{unit} - for Aluminum and CFRP $[0_4]$

Figure 15: Load case 2 normalized apparent stiffnesses versus L_x and n_{unit} - for CFRP $[90_4]$ and CFRP $[\pm 45]_s$

to the stiffness predicted of the inner solution as calculated by homogenization models. For isotropic materials with Poisson's ratios of $\nu = 0.3$ or smaller the deviations are at maximum 15 percent. The highest deviations occur with the angle-ply laminate where Poisson's ratio reaches $\nu_{xy} = 0.875$. However, if the distance between the clamps is equal to or greater than the width along the corrugations, the apparent stiffness of corrugated (!) sheets matches accurately $\tilde{A}_{11}$ as calculated by the homogenization models.

5.2 Load case 2: strain in the direction of corrugations

For this load case, the clamping length L_x as well as the number of unit cells n_{unit} has an influence on the normalized stiffness. The corresponding stiffness maps can be found in Figures 14 and 15, sorted by materials and lay-ups. This load case has shown a higher sensitivity to the number of elements in the direction of corrugations, wherefore this parameter needed to be increased for the given simulations.

5.2.1 Influence of out-of-plane length

For the given investigation, the distance between the clamps is fixed with P whereas the width L_x of the clamps changes.
In case of plates, edge effects are relevant at low clamp widths. It is therefore that the trends of stiffness evolution with L_x seen here are the opposite to those seen in load case 1. All flat sheets approach the plate stiffness A_{22} predicted by homogenization methods with increasing clamp width. With narrow clamps the respective Young's moduli are approached.
In comparison with flat plates, the clamping length only seems to have a minor effect on the normalized stiffness of corrugated sheets and laminates, as can be concluded from the nearly straight level lines in Figures 14 and 15. Only corrugated laminates with the $[\pm 45]_s$ lay-up show a high clamping length sensitivity due to the said effect of the high Poisson's ratio. Global extension along the corrugations is kinematically connected with local bending κ_{yy}, which in return is elastically coupled with bending in the other direction. The bottom diagram in Figure 15 reveals a very high loss of extensional stiffness if the clamp width is not significantly larger than the length P. This effect is, again, due the high Poisson's ratio of the laminate $[\pm 45]_s$.

5.2.2 Influence of number of unit cells

Figures 14 and 15 reveal that the apparent stiffness of the corrugated sheets or laminates is usually higher than what the homogenization models obtain if only a low number of unit cells is considered. This is due to the fact that the clamps prevent rotation about the x direction, resulting in a stiffening effect due to the additionally constrained degree of freedoms. If a larger number of unit cells is considered, the realistic stiffness is quite accurately predicted by $\tilde{A}_{22}$ of the homogenization models for the aluminum sheet and both unidirectional laminates.
In case of the $[\pm 45]_s$ corrugated laminates, the stiffening effect of the clamps at low unit cell numbers is only visible at large values of clamping length since the behavior at short lengths is governed by the Poisson's ratio (see the considerations in section 5.2.1).

5.3 Load case 3: in-plane shear

For this load case homogenization models describe an inner solution assuming that shear stresses $\tau_{xs} = \tau_{sx}$ remain constant along x. As the un-clamped edges $\pm L_x/2$ must satisfy free-edge boundary conditions, all stresses σ_{xi} must vanish there.

5.3.1 Influence of out-of-plane length

The top and bottom diagrams in Figures 16 and 17 reveal that the apparent shear stiffness vanishes at small clamp width values for all laminates and corrugation amplitudes. In order to show that the homogenization-model predictions are recovered at high clamp widths, the clamp-width range - corresponding to the out-of-plane length L_x - was extended to a high value one order of magnitude higher than in all other diagrams.
Independent of laminate design, flat sheets retain higher shear stiffness than corrugated laminates from where it can be concluded that edge effects increases with increasing corrugation amplitude.
Base-sheet, or laminate-design, show an influence on the given observation, which can be identified by comparing the shift of the level lines with respect to the clamp width of the different material configurations. Clearly, the direction of anisotropy has an influence: the unidirectional laminate $[0_4]$ (see Figure 16) shifts the lines towards higher clamp width, whereas the unidirectional laminate $[90_4]$ (displayed in Figure 17) shifts the lines towards lower clamp width, as compared to the isotropic material whose

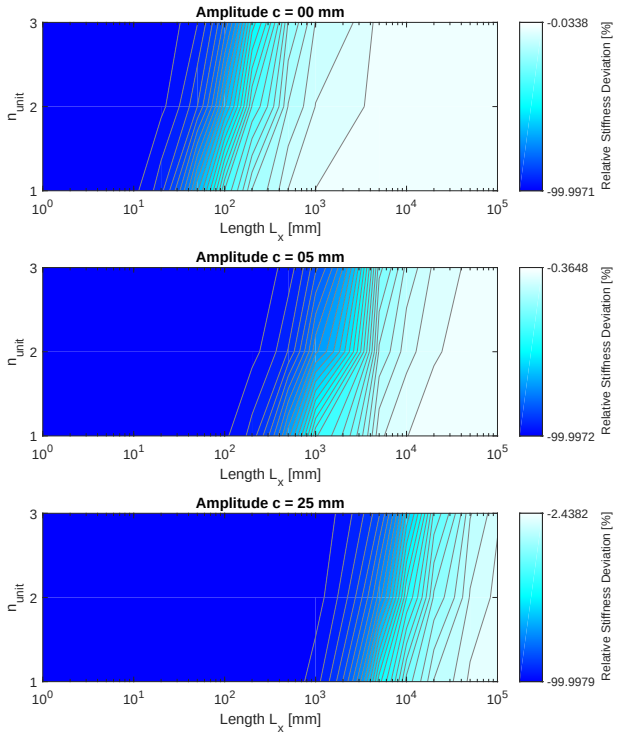

(a) Aluminum

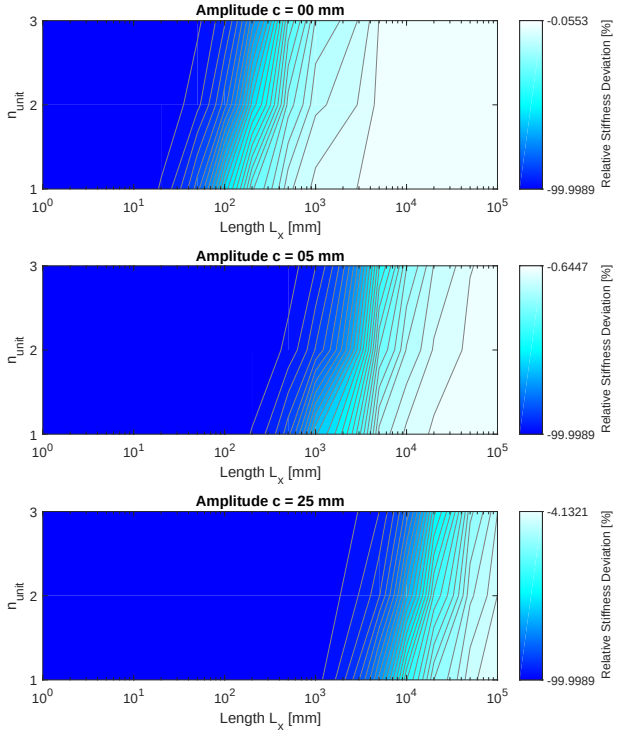

(b) CFRP $[0_4]$

Figure 16: Load case 3 normalized apparent stiffnesses versus L_x and n_{unit} - for Aluminum and CFRP $[0_4]$

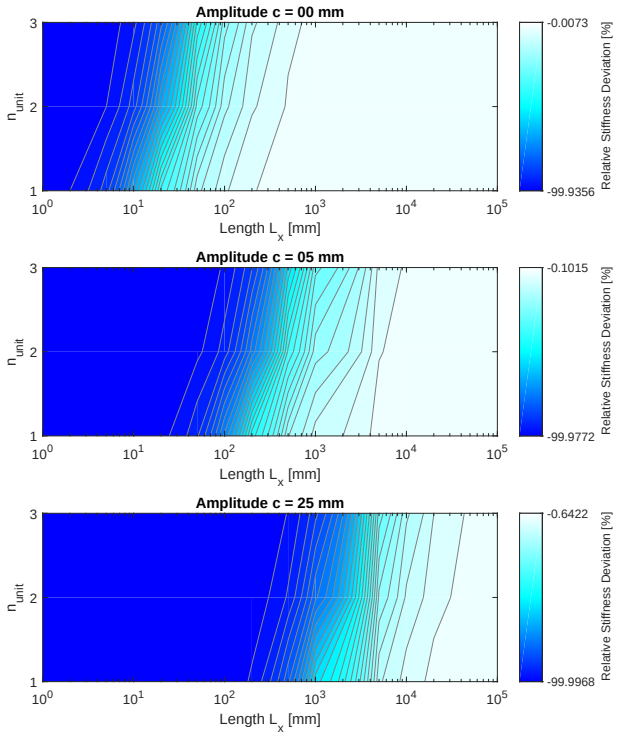

(c) CFRP $[90_4]$

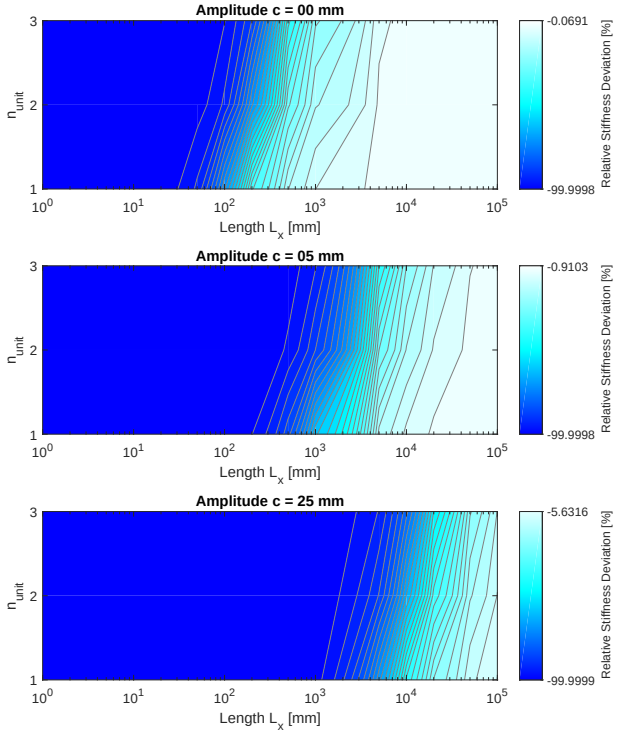

(d) CFRP $[\pm 45]_s$

Figure 17: Load case 3 normalized apparent stiffnesses versus L_x and n_{unit} - for CFRP $[90_4]$ and CFRP $[\pm 45]_s$

curves shown with the diagram in Figure 16. The different behavior of the two unidirectional laminates is also interesting when keeping in mind that they both have the same value of homogenized shear stiffness $\tilde{A}_{66}$. The largest edge effects in terms of stiffness deviation are seen for the laminate $[\pm 45]_s$, see Figure 17, where the homogenization-model prediction $\tilde{A}_{66}$ is not reached even at the high plate-aspect ratio $L^\star = 1000$.

5.3.2 Influence of number of unit cells

Figures 16 and 17 reveal that increasing the number of unit cells leads to an increase in the minimum required clamping width needed for reaching the homogenization model stiffness $\tilde{A}_{66}$ which implies a dependence on the aspect ratio $L^\star$. Hence, the peculiarities seen in this load case do not vanish if n_{unit} is increased.

5.4 Load case 4: bending about the corrugated direction

In this case as well, the number of unit cells is fixed to one, as the influence on the results is minor. It needs to be noted that for reasons of numerical stability, shell elements were used for obtaining the plate solutions displayed in Figure 18.

The trends seen in bending κ_{xx} are the same as seen in load case 1, where the strain ε^0_{xx} is applied. The isotropic reference as well as all laminates show a clamping effect for short out-of-plane lengths L_x in presence of a corrugation amplitude. For the unidirectional laminates shown in Figures 18b) and 18c) the calculated stiffness values are very close to the predictions obtained using the homogenization model. Even for the corrugated laminates $[\pm 45]_s$, see Figure 18d), good agreement with $\tilde{D}_{11}$ is reached for larger lengths $L_x \geq 100$.

5.5 Load case 5: bending transverse to the corrugated direction

Similarly to load case 2, the convergence study for the given simulations has shown a higher sensitivity to the number of elements in the corrugated direction. As a consequence, this parameter was increased compared to the other load cases.

The results presented in Figures 19 and 20 show a strong reduction of the bending stiffness compared to the unit

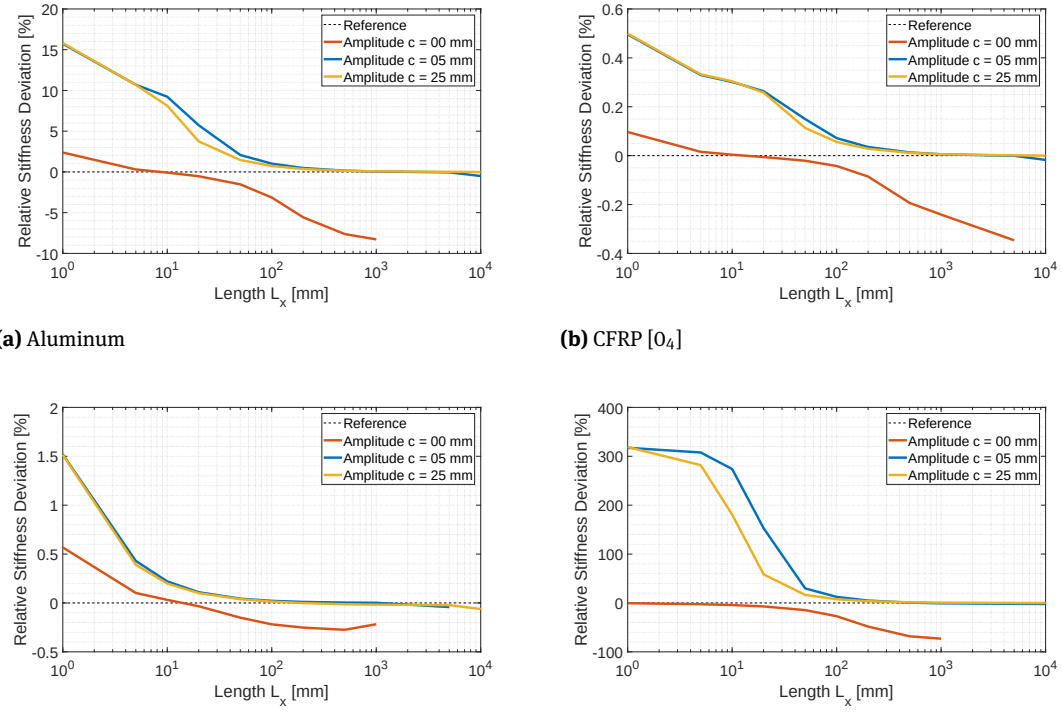

(a) Aluminum

(b) CFRP $[0_4]$

(c) CFRP $[90_4]$

(d) CFRP $[\pm 45]_s$

Figure 18: Load case 4 normalized apparent stiffnesses versus L_x

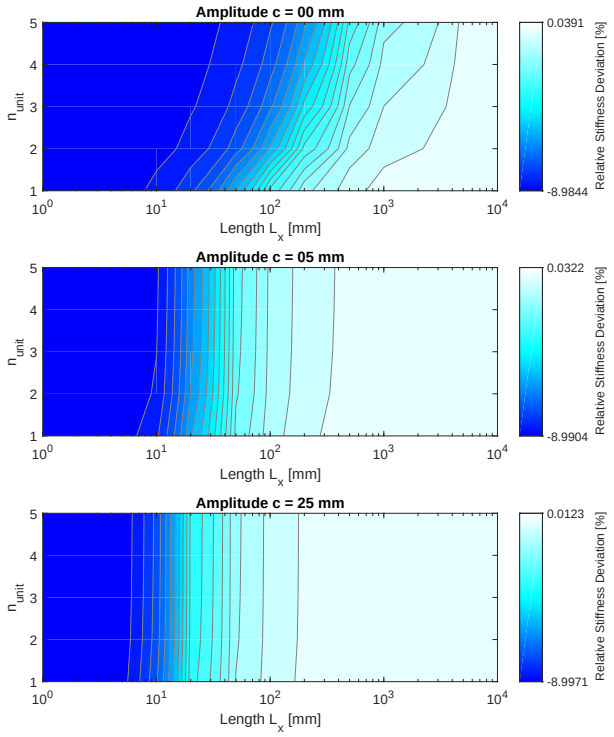

(a) Aluminum

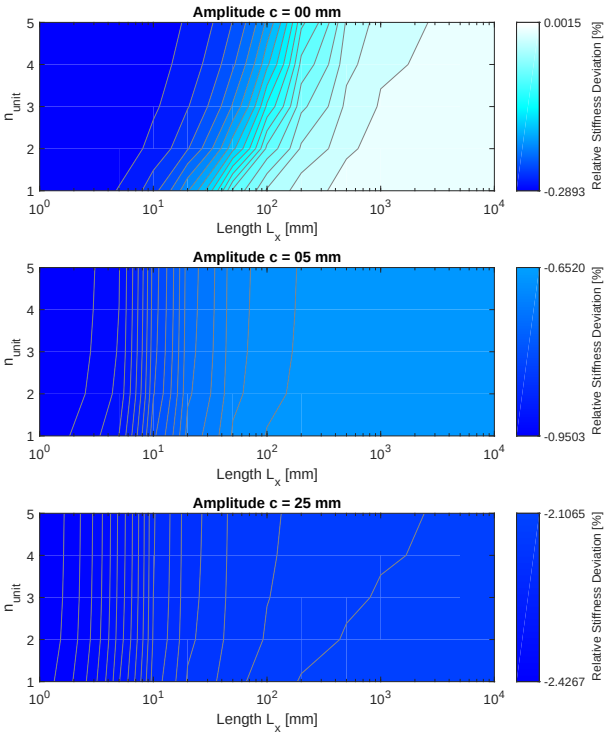

(c) CFRP $[90_4]$

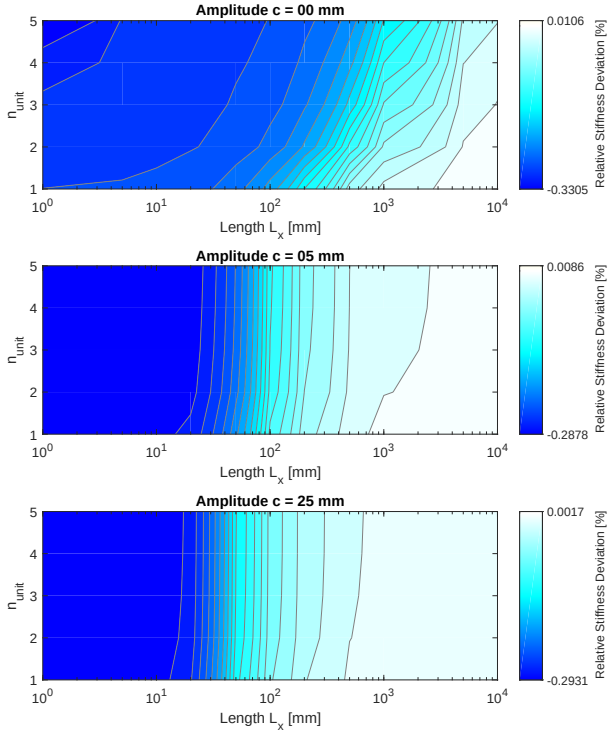

(b) CFRP $[0_4]$

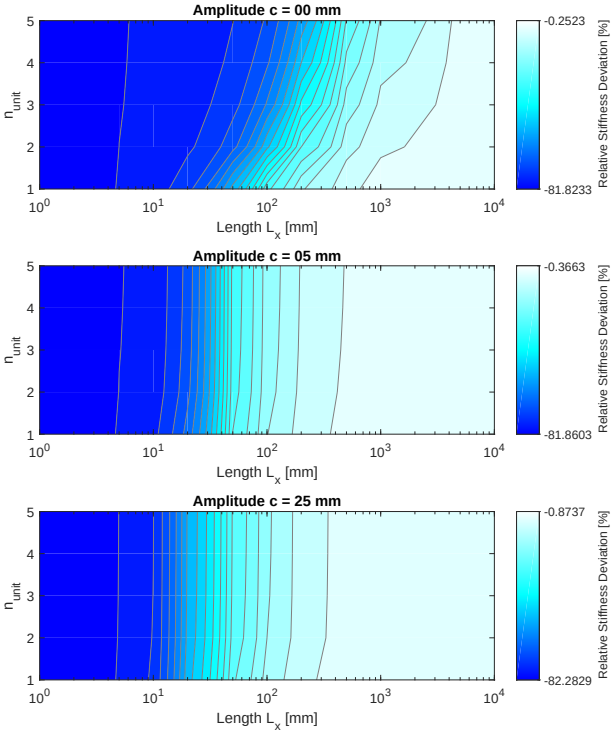

(d) CFRP $[\pm 45]_s$

Figure 19: Load case 5 normalized apparent stiffnesses versus L_x and n_{unit} - for Aluminum and CFRP $[0_4]$

Figure 20: Load case 5 normalized apparent stiffnesses versus L_x and n_{unit} - for CFRP $[90_4]$ and CFRP $[\pm 45]_s$

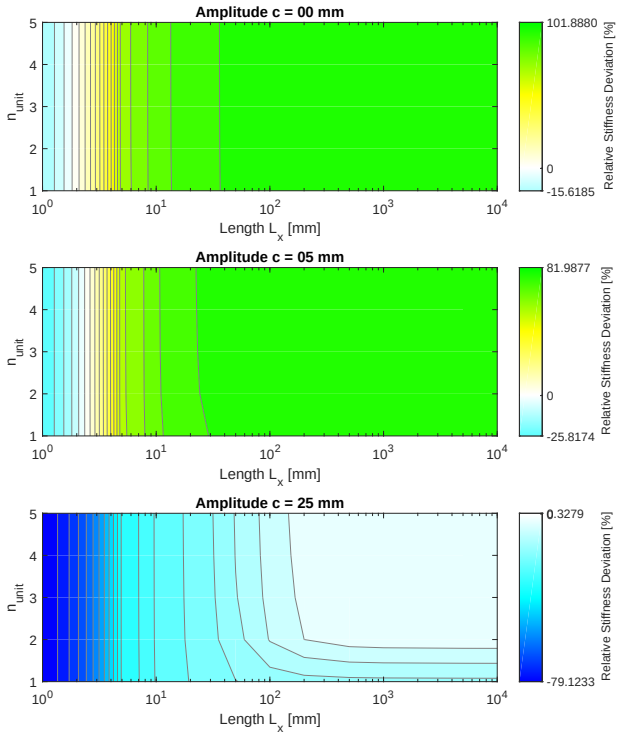

(a) Aluminum

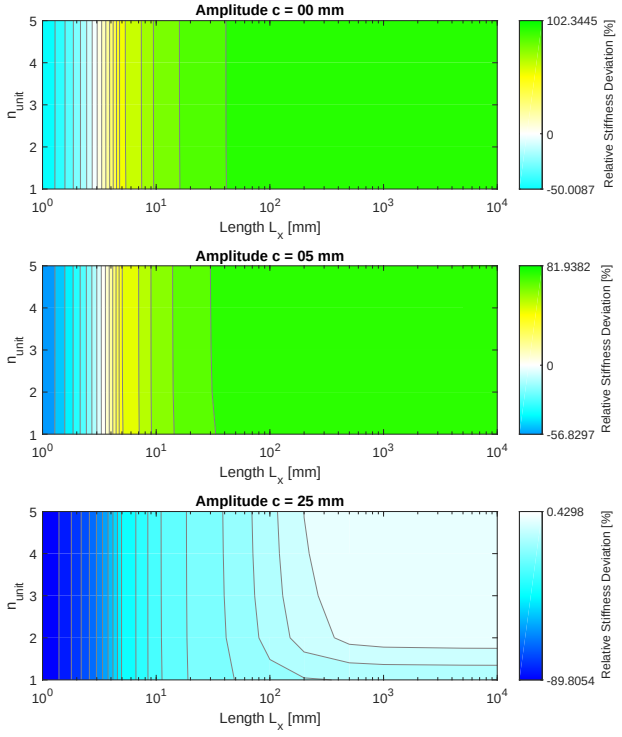

(b) CFRP $[0_4]$

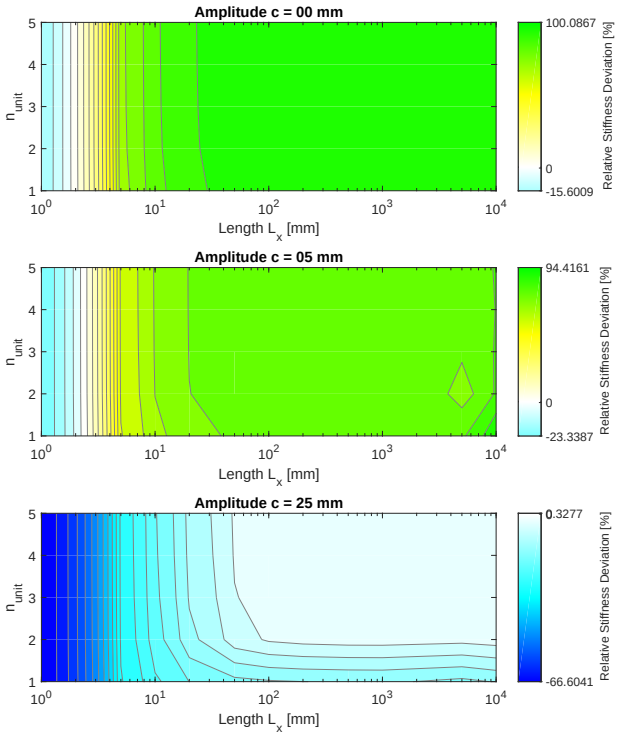

(c) CFRP $[90_4]$

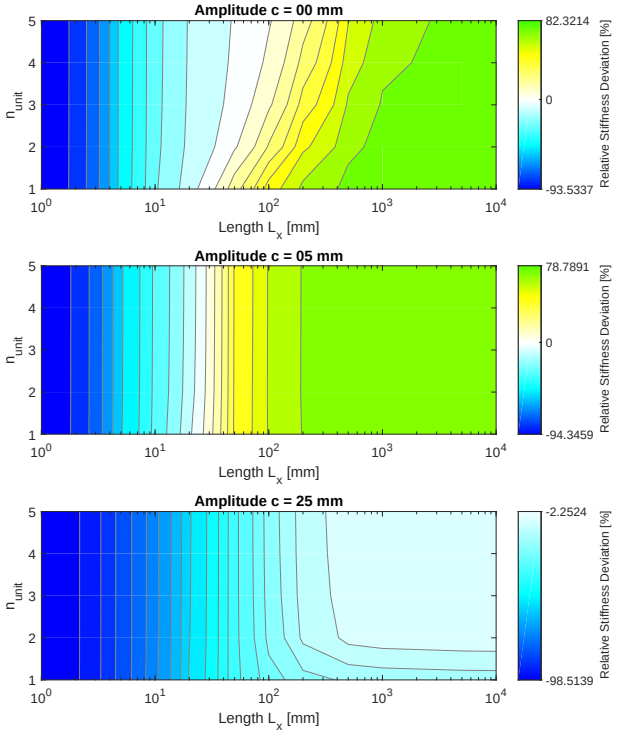

(d) CFRP $[\pm 45]_s$

Figure 21: Load case 6 normalized apparent stiffnesses versus L_x and n_{unit} - for Aluminum and CFRP $[0_4]$

Figure 22: Load case 6 normalized apparent stiffnesses versus L_x and n_{unit} - for CFRP $[90_4]$ and CFRP $[\pm 45]_s$

cell value for small clamp widths L_x. The intensity of the deviation can be observed to be proportional to the material's averaged Poisson's ratio, as the effect is much more pronounced for the $[\pm 45]_s$ laminate. The latter once again loses much of its bending stiffness for small values of L_x. Larger clamp-width values let the inner solution, which describes cylindrical bending, dominate so that the stiffness under realistic conditions approaches $\tilde{D}_{22}$ at clamping widths $L_x \geq 100$.
Note that the diagrams also indicate that the influence of the number of unit cells is less pronounced for the corrugated examples.

5.6 Load case 6: torsion

The stiffness maps displayed in Figures 21 and 22 indicate that in case of plates with a sufficient out-of-plane length L_x, a torsional stiffness deviation of 100%, hence twice the stiffness D_{66} predicted by the inner solution, is reached - regardless of the material used. Similarly, a reduction of the calculated stiffness is visible for short values of L_x.
In contrast to the behavior seen in the results of the plates, corrugated sheets with a corrugation amplitude of $c = 25\ mm$ show no remarkable stiffness deviation at large values of L_x. Only a small influence of the number of unit cells as well as a reduced stiffness for short out-of-plane lengths can be identified. Similar observations can be made for $c = 5\ mm$.
In accordance with the aforementioned observations, sheets and laminates with a corrugation amplitude of $c = 5\ mm$ and large dimensions show a maximum stiffness deviation of 60% – 80%, which is between the values for the plate (factor 2) and the semi-circular corrugated structure (factor 1).

6 Discussion

6.1 Load cases with fast decay of boundary effects

The majority of the load cases presented in this study show a fast decay of the effects caused by the load introduction (clamping) on the relative stiffness of corrugated structures.

For both load cases 1 and 4, the clamps show a stiffening effect for small out of-plane lengths L_x. For $L_x \geq 1000\ mm$ the stiffness agrees well with the values calculated with the homogenization model. In these load cases, only one unit cell with a width of $P = 100\ mm$ is considered, hence, the interior solution is already accurate for a minimum length of ten times that of the unit cell.

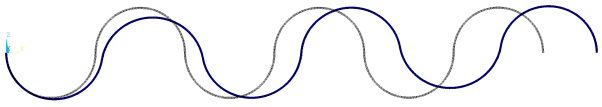

(a) Clamped boundary condition

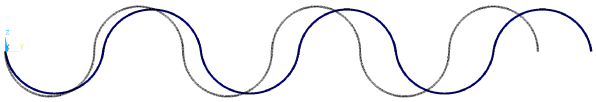

(b) Simply supported boundary condition

Figure 23: Scaled displacement of a corrugated panel subjected to loading in the direction of corrugation (LC 2). The plots highlight the influence of support conditions on the resulting deformation.

For load case 2 the stiffening effect of the clamps is visible if the number of corrugations is low. Note that the given selection of boundary conditions with clamps represents the upper bound of edge constraints. Additionally, it has been shown to induce axial and bending coupling [59]. In the given implementation, vertical deflection of the corrugated panel is impeded at both end supports due to the chosen displacement boundary conditions. As a consequence, a reaction moment at the clamping is induced, which contributes to the stiffening effect and also has an an influence on the resulting deformation. This is shown in Figure 23, where the relation between support conditions and the resulting displacements is visualized. If the panel is clamped (Subplot 23a)), the induced vertical deflection in the left and right part of the structure is of opposite sign, whereas there is no out-of-plane displacement in the center part of the laminate due to reasons of symmetry. If the panel is simply supported at the midplane (Subplot 23b)) instead, the vertical displacement is uniformly distributed in all areas and no additional bending is induced. As a consequence, the influence of edge effects on structural stiffness is also less pronounced.

6.2 Load case 3: corrugated laminates subjected to in-plane shear loading

The in-plane shear load case has shown to be really sensitive to boundary effects. As can be seen in Figures 16 and 17 there is a large range of the out-of-plane length L_x where

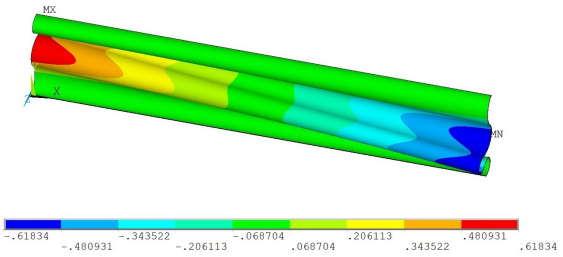

(a) $L_x = 1000\ mm$, $\frac{A_{66}}{\tilde{A}_{66}} = 0.23$, $n_{unit} = 2$

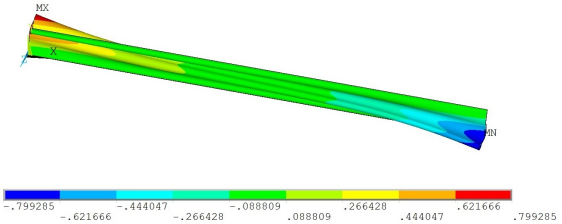

(b) $L_x = 3000\ mm$, $\frac{A_{66}}{\tilde{A}_{66}} = 0.66$, $n_{unit} = 2$

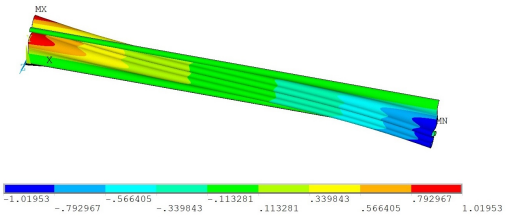

(c) $L_x = 3000\ mm$, $\frac{A_{66}}{\tilde{A}_{66}} = 0.52$, $n_{unit} = 3$

Figure 24: Scaled deformation of different corrugated laminates with CFRP $[90_4]$ lay-up and 1 mm thickness subjected to shearing. The color bar indicates the deformation in y-direction (in-plane deformation).

basically no stiffness $\tilde{A}_{66}$ at all is detected. The problem intensifies if the number of unit cells is increased, hence implying a dependency on the aspect ratio L^*.

Figure 24 shows the resulting deformation of several corrugated laminates with different geometric parameters subjected to shear loading. As can be clearly seen, the free edges exhibit displacements both in in-plane- and in out-of-plane-direction. These kinds of deformations lower the effective shear stiffness of corrugated laminates. They are more likely to occur for structures with a high corrugation amplitude, which explains the increase of the critical length L_x^{crit} with increasing amplitude, seen in all cases in Figures 16 and 17.

The homogenization model used for providing the interior solution stiffness value $\tilde{A}_{66}$ assumes that the corrugated laminate is subjected to a shear strain ϵ_{xy} only. Such a state of deformation is only found in the green area in the middle of the laminates seen in Figure 24. Increasing the length L_x causes the respective area to grow and the stiffness to increase, while adding unit cells increases the free-edge effects and leads to a reduction in shear stiffness.

The fact that corrugated laminates show a relatively low in-plane shear stiffness in a large range of geometry is not necessarily a drawback from a structural point of view - it can be exploited where needed. Hence, we e.g. propose the use of said structures as bearing or damping elements.

6.3 Load case 6: corrugated laminates subjected to torsional loading

The results presented in section 5.6 show that the torsional stiffness of finite-width plates is twice the value calculated using the classical theory of laminated plates (CLPT). As can be seen in Figure 25, interlaminar shear stresses can be found in finite-width plates as a result of the free edges.

Whitney [81] thoroughly investigated the influence of transverse shear and plate thickness on anisotropic plates subjected to torsional loading by introducing a modified shear deformation theory. He used CLPT as a benchmark, however, modified with a correction factor as it can be shown that transverse shear contributes half to the resulting torque in case of homogeneous lay-ups. As a result, the stiffness doubles:

$$D_{66}^{actual} = 2 \cdot D_{66}^{CLPT}\ . \tag{33}$$

Note that Equation 33 is only valid for thin laminates as the distribution of transverse shear stresses shows a large dependency on the plate thickness [81, 82]. In the given case, a correction factor of 2 has shown to be valid for a thickness of $t = 1\ mm$ (as used in the numerical study), whereas the correction factor has reduced to 1.874 for the example shown in Figure 25, where the plate thickness is $t = 10\ mm$.

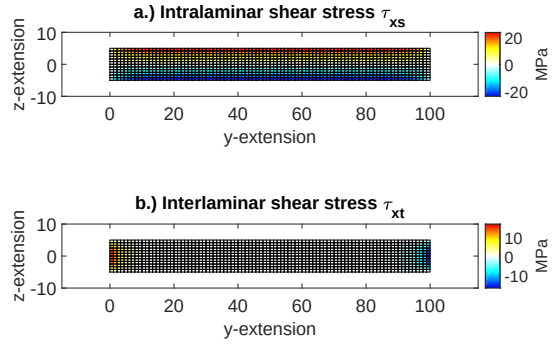

(a) Plate with finite width

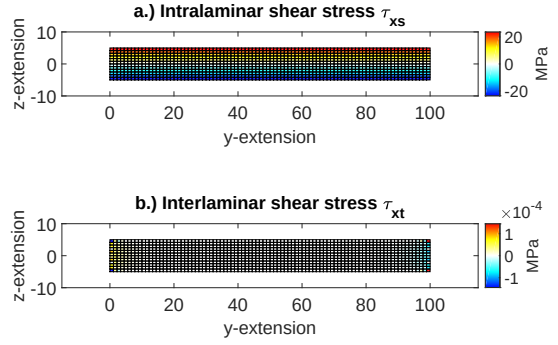

(b) Plate with infinite width (as in CLPT)

Figure 25: Shear stress distribution in a CFRP $[0_4]$ laminate subjected to torsional loading. For better visibility, we have increased the laminate thickness to $t = 10\ mm$. The results for the finite-width plates were produced using the code presented in [62] with deactivated periodicity boundary condition.

The results of the parameter study indicate that the torsional stiffness of corrugated laminates approaches the unit-cell value as the amplitude is increased.

Figure 26 shows the shear-stress distribution in a semi-circular corrugated laminate consisting of one unit cell. As in case of the plate, the presence of free edges leads to interlaminar shear stresses. For the given configuration the value of the local interlaminar stress τ_{xt} is maximum at the free edges ($z = 0$) where it corresponds to τ_{xy}. The contribution of the interlaminar stresses to the total torque can then be estimated as follows:

$$T_{intralaminar} = \int_A (\tau_{xz} \cdot y - \tau_{xy} \cdot z)\, dA \approx -\int_A \tau_{xy} \cdot z\, dA \approx 0\,. \tag{34}$$

Hence, the free edges do not affect the torsional stiffness $\tilde{D}_{66}$ in case of a semi-circular corrugation shape. This is also seen in Figure 27, where the evolution of the correction factor for a thin CFRP $[0_4]$ laminate with increasing corrugation amplitude is shown. Note that for a laminate

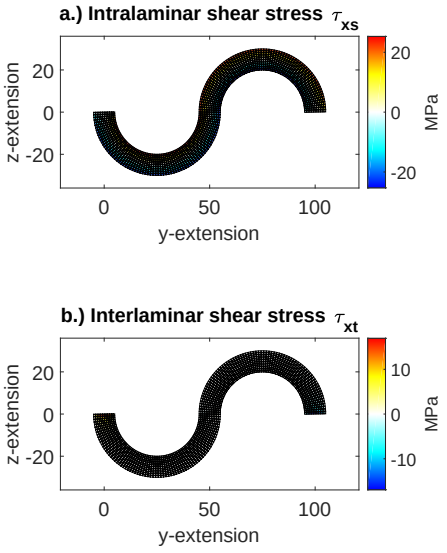

Figure 26: Shear stress distribution in a CFRP $[0_4]$ semi-circularly corrugated laminate subjected to torsional loading. For better visibility, the laminate thickness was increased to $t = 10\ mm$. The results for the finite-width plates were produced using the code presented in [62] with deactivated periodicity boundary condition.

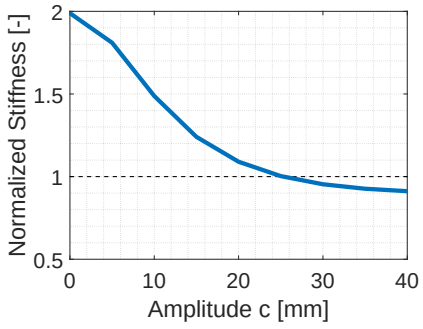

Figure 27: Evolution of the normalized stiffness $D_{66}^{actual} \cdot (D_{66}^{CLPT})^{-1}$ with increasing corrugation amplitude. The lay-up is CFRP $[0_4]$, with a total thickness of $t = 1\ mm$ and a unit cell width of $P = 100\ mm$. The results for the finite-width plates were produced using the code presented in [62] with deactivated periodicity boundary condition.

with an even larger corrugation amplitude ($c > 0.25 \cdot P$) the torsional stiffness of the laminate with finite width actually drops below the unit cell value.

7 Conclusion

In order to reduce the numerical cost, the structural response of corrugated laminates is often calculated using homogenization models, which provide substitute plate

properties of the given structure. As they assume periodicity of the state variables - which is usually enforced by applying periodicity boundary conditions - they are used to calculate the interior solution, which only maps the global behavior of the structures. Thus, any edge effects, e.g. caused by the supports or by free edges, are not considered. In order to establish the range of validity of homogenization models we have therefore performed a numerical study which provides insight on the influence of clamping and free edge effects on the structural stiffness.

In most load cases the influence of edge effects remains limited to a small range of geometrical parameters which may hardly ever be used in practical applications. In contrast to that, the in-plane shear stiffness of corrugated laminates has shown to be highly influenced by free-edge effects. The latter show a strong dependency on the geometrical parameters: they become more dominant if the corrugation amplitude is increased and/or the aspect ratio of the corrugated sheet is reduced. As a result, the actual shear stiffness is smaller than the corresponding inner solution value in a large range of geometry. Hence, the use of homogenization models in case of the given loading situation is problematic and should be examined from case to case.

Similarly to the case of plates, the torsional stiffness of corrugated laminates is influenced by interlaminar shear stresses at the free edges. The deviation is maximum for the plate (up to a factor of two for thin laminates) and reduces as the corrugation amplitude is increased. For semicircular corrugated laminates the stiffness offset vanishes, which is a result of the peculiar geometry.

In general, the study has shown that homogenization models perform quite well in a large part of the investigated cases. Regarding the exceptions and peculiarities identified, the present work may serve as a guideline for assessing their influence on structural stiffness.

Acknowledgement: The authors gratefully acknowledge the support of the Swiss National Science Foundation (project no. 169468 and grant no. 200021_169468 / 1).

References

[1] Junkers H., Flying-machine supporting surface, 1923, US Patent No.14627.
[2] Junkers H., Corrugated sheet metal, 1924, US Patent No. 1517633.
[3] Junkers H., Flying-machine covering, 1925, US Patent No. 1553695.
[4] Junkers H., Corrugated sheet-metal shape, 1929, US Patent No. 704326.
[5] Mornement A., Holloway, S., Corrugated Iron - Builing on the Frontier, 2007, Francis Lincoln Limited, London, UK.
[6] Thurnherr C., Ruppen L., Kress G., Ermanni, P., Interlaminar Stresses in Corrugated Laminates, Compos. Struct., 2016, 140, 296-308.
[7] Thurnherr C.N., Ruppen L., Kress G., Ermanni P., Non-linear Stiffness Response of Corrugated Laminates in Tensile Loading, Compos. Struct., 2016, 157, 244-255.
[8] Thurnherr C.N., Ruppen L., Brändli S., Franceschi C., Kress G., Ermanni P., Stiffness Analysis of Corrugated Laminates under Large Deformation, Compos. Struct., 2017, 160, 457-467.
[9] Bai J. B., Chen D., Xiong J.J., Dong C.H., A semi-analytical model for predicting nonlinear tensile behaviour of corrugated flexible composite skin, Compos. Part B: Eng., 2019, 168, 312-319.
[10] Kress G.R., Filipovic D.T., An analytical nonlinear morphing model for corrugated laminates, Curved and Layer. Struct., 2019, 6, 57-67.
[11] Soltani Z., Kordkheili S.A., Kress G., Experimental and numerical study of geometrically nonlinear behavior of corrugated laminated composite shells using a nonlinear layer-wise shell fe formulation, Eng. Struct. 184, 2019, 61-73.
[12] Thurnherr C.N., Pedergnana T., Kress G, Ermanni P., Non-Classical Vibration Behavior of Highly Anisotropic Corrugated Laminates, Compos. Struct. 168, 2017, 84-91.
[13] Malikan M., Dimitri R., Tornabene F., Effect of sinusoidal corrugated geometries on the vibrational response of viscoelastic nanoplates, Appl. Sci., 2018, 8(9), 1432.
[14] Nguyen-Minh N., Tran-Van N., Bui-Xuan T., Nguyen-Thoi T., Free Vibration Analysis of Corrugated Panels Using Homogenization Methods and a Cell-Based Smoothed Mindlin Plate Element, CSMIN3), Thin. Wall. Struct., 2018, 124, 184-201.
[15] Filipovic D.T., Kress G.R., A planar finite-element formulation for corrugated laminates under transverse shear load, Compos. Struct., 2018, 201, 958-967.
[16] Filipovic D., Kress G., Manufacturing method for high-amplitude corrugated thin-walled laminates, Compos. Struct., 2019, 222, 110925.
[17] Dayyani I., Shaw A.D., Saavedra Flores E., Friswell M. I., The mechanics of composite corrugated structures: a review with applications in morphing aircraft, Compos. Struct. 2015, 133, 358-380.
[18] Friswell M.I., Morphing aircraft: An improbable dream?, in: Proc. ASME Conf. Smart Mater., Adaptive Structures and Intelligent Systems SMASIS2014, Newport, Rhode Island, USA, 2014, V001T08A001.
[19] Ajaj R.M., Beaverstock C.S., Friswell M.I., Morphing aircraft: The need for a new design philosophy, Aerosp. Sci. Technol., 2016, 49, 154-166.
[20] Li D., Zhao S., Da Ronch A., Xiang J., Drofelnik J., Li Y., Zhang L., Wu Y., Kintscher M., Monner H.P., Rudenko A., Guo S., YinW., Kirn J., Storm S., De Breuker R., A review of modelling and analysis of morphing wings, Prog. Aerosp. Sci., 2018, 100, 46-62.
[21] Thill C., Etches J., Bond I., Potter K., Morphing skins, Aeronaut. J., 2008, 112(1129), 117-139.
[22] Thill C., Etches J.A., Bond I.P., Potter K.D., Weaver P.M., Corrugated composite structures for aircraft morphing skin applications, in:, Ed. 18th Int. Conf. of Adaptive Structures and Technologies, Ottawa, Ontario, Canada, 2007, 134, 507-514.
[23] Gandhi F., Anusonthi P., Skin design studies for variable camber morphing airfoils, Smart. Mater. Struct., 2008, 17, 1-8.

[24] Airoldi A., Sala G., Di Landro L.A., Bettini P., Gilardelli A., Composite Corrugated Laminates for Morphing Applications, in: Antonio Concilio, Ignazio Dimino, Leonardo Lecce, Rosario Pecora, Ed., Morphing Wing Technologies, Butterworth and Heinemann, Oxford, 2018, 9, 247-276.
[25] Previtali F., Molinari G., Arrieta A.F., Guillaume M., Ermanni P., Design and Experimental Characterization of a Morphing Wing with Enhanced Corrugated Skin, J. Intell. Mat. Syst. Str., 2016, 27(2), 278-292.
[26] Takahashi H., Yokozeki T., Hirano Y., Development of Variable Camber Wing with Morphing Leading and Trailing Sections Using Corrugated Structures, J. Intell. Mat. Syst. Str., 2016, 27(20), 2827-2836.
[27] Bai J.B., Chen D., Xiong J.J., Shenoi R.A., A Corrugated Flexible Composite Skin for Morphing Applications, Compos. Part B: Eng., 2017, 131, 134-143.
[28] Henry A.C., Molinari G., Rives-Padilla J.R., Arrieta A.F., Smart morphing wing: Optimization of distributed piezoelectric actuation, AIAA J., 2019, 254.
[29] Gong X., Liu L., Scarpa F., Leng J., Liu Y., Variable stiffness corrugated composite structure with shape memory polymer for morphing skin applications, Smart Mater. Struct., 2017, 26, 035052.
[30] Thurnherr C., Mirabito Y., Kress G., Ermanni P., Highly Anisotropic Corrugated Laminates Deflection under Uniform Pressure, Compos. Struct., 2016, 154, 31-38.
[31] Ermakova A., Dayyani I., Shape optimisation of composite corrugated morphing skins, Compos. Part B: Eng., 2017, 115, 87-101.
[32] Shaw A.D., Dayyani I., Friswell M.I., Optimisation of Composite Corrugated Skins for Buckling in Morphing Aircraft, Compos. Struct., 2015, 119, 227-237.
[33] Thill C., Downsborough J.D., Lai S.J., Bond I.P., Jones D.P., Aerodynamic study of corrugated skins for morphing wing applications, Aeronaut. J., 2010, 3407, 237-244.
[34] Xia Y., Bilgen O., Friswell M.I., The effect of corrugated skins on aerodynamic performance, J. Intell. Mat. Syst. Str. 2012, 25(7), 786-794.
[35] Dayyani I., Ziaei-Rad S., Friswell M.I., The mechanical behavior of composite corrugated core coated with elastomer for morphing skins, J. Compos. Mater., 2014, 48(13), 1623-1636.
[36] Dayyani I., Friswell M.I., Multi-objective optimization for the geometry of trapezoidal corrugated morphing skins, Struct. Multidiscip. O. 2017, 55(1), 331-345.
[37] Ren Y., Jiang H., Ji W., Zhang H., Xiang J., Yuan F.-G., Improvement of progressive damage model to predicting crashworthy composite corrugated plate, Appl. Compos. Mater., 2018, 25(1), 45-66.
[38] Ren Y., Jiang H., Gao B., Xiang J., A progressive intraply material deterioration and delamination based failure model for the crashworthiness of fabric composite corrugated beam: Parameter sensitivity analysis, Compos. Part B: Eng., 2018, 135, 49-71.
[39] Ren Y., Zhang H., Xiang J., A novel aircraft energy absorption strut system with corrugated composite plate to improve crashworthiness, Int. J. Crashworthines, 2018, 23(1), 1-10.
[40] Buannic N., Cartraud P., Quesnel T., Homogenization of corrugated core sandwich panels, Compos. Struct., 2003, 59, 299-312.
[41] Aboura Z., Talbi N., Allaoui S., Benzeggagh M.L., Elastic behavior of corrugated cardboard: experiments and modeling, Compos. Struct., 2004, 63(1), 53-62.
[42] Biancolini M.E., Evaluation of equivalent stiffness properties of corrugated board, Compos. Struct., 2005, 69(3), 322-328.
[43] Talbi N., Batti A., Ayad R., Guo Y.Q., An analytical homogenization model for finite element modelling of corrugated cardboard, Compos. Struct., 2009, 88(2), 280-289.
[44] Kazemahvazi S., Zenkert D., Corrugated all-composite sandwich structures. part 1: Modeling, Compos. Sci. Technol., 2009, 69(7-8), 913-919.
[45] Kazemahvazi S., Tanner D., Zenkert D., Corrugated all-composite sandwich structures. part 2: Failure mechanisms and experimental programme, Compos. Sci., Technol., 2009, 69(7-8), 920-925.
[46] Abbčs B., Guo Y.Q., Analytic homogenization for torsion of orthotropic sandwich plates: Application to corrugated cardboard, Compos. Struct., 2010, 92(3), 699-706.
[47] Dayyani I., Friswell M.I., Ziaei-Rad S., Equivalent models of composite corrugated cores with elastomeric coatings for morphing structures, Compos. Struct., 2013, 104, 281-292.
[48] Bartolozzi G., Pierini M., Orrenius U., Baldanzini N., An equivalent material formulation for sinusoidal corrugated cores of structural sandwich panels, Compos. Struct., 2013, 100, 173-185.
[49] Bartolozzi G., Baldanzini N., Pierini M., Equivalent properties for corrugated cores of sandwich structures: A general analytical method, Compos. Struct., 2014, 108, 736-746.
[50] Cheon Y.-J., Kim H.-G., An Equivalent Model for Corrugated Sandwich Panels, J. Mech. Sci. Technol. 29, 3„ 2015, 1217-1223.
[51] Isaksson P., Carlson L.A., Analysis of the Out-Of-Plane Compression and Shear Response of Paper-based Web-Core Sandwiches Subject to Large Deformation, Compos. Struct., 2017, 159, 96-109.
[52] Briassoulis D., Equivalent Orthotropic Properties of Corrugated Sheets, Comput. Struct., 1986, 23(2), 129–138.
[53] Shimansky R.A., Lele M.M., Transverse Stiffness of a sinusoidally corrugated plate, Mech. Struct. Mech., 1995, 23(3), 439-451.
[54] Yokozeki T., Takeda S.-T., Ogasawara T., Ishikawa T., Mechanical properties of corrugated composites for candidate materials of flexible wing structures, Compos. Part A: Appl. S., 2006, 37, 1578-1586.
[55] Kress G., Winkler M., Corrugated Laminate Homogenization Model, Compos. Struct., 2010, 92,(3), 795-810.
[56] Xia Y., Friswell M.I., Equivalent models of corrugated laminates for morphing skins, in: Active and Passive Smart Structures and Integrated Systems 2011, Proc. Vol. 7977 of SPIE Smart Structures and Materials + Nondestructive Evaluation and Health Monitoring, SPIE, San Diego, California, USA, 2011, 79771I
[57] Xia Y., Flores E.I.S., Friswell M.I., Equivalent Models of Corrugated Panels, Int. J. Solids. Struct., 2012, 49(13), 1453-1462.
[58] Mohammadi H., Ziaei-Rad S., Dayyani I., An Equivalent Model for Trapezoidal Corrugated Cores Based on Homogenization Method, Compos. Struct., 2015, 131, 160-170.
[59] Wang C., Khodaparast H.H., Friswell M.I., Shaw A.D., An equivalent model of corrugated panels with axial and bending coupling, Comput. Struct., 2017, 183, 61-72.
[60] Nguyen-Minh N., Tran-Van N., Bui-Xuan T., Nguyen-Thoi T., Static Analysis of Corrugated Panels Using Homogenization Models and a Cell-Based Smoothed Mindlin Plate Element (CS-MIN3), Front. Struct. Civil Eng., 2018, https://doi.org/10.1007/s11709-017-0456-0).
[61] Moro A., Filipovic D., Kress G., Winkler M., Thin-shell-theory solutions for the static structural response of circular-sections shaped corrugated laminates, Compos. Struct., 2020, 236, 111730.

[62] Kress G., Winkler M., Corrugated Laminate Analysis: A Generalized Plane-Strain Problem , Compos. Struct., 2011, 93, 1493-1504.
[63] Park K.-J., Jung K., Kim Y.-W., Evaluation of Homogenized Effective Properties for Corrugated Composite Panels, Compos. Struct., 2016, 140, 644-654.
[64] Aoki Y., Maysenhölder W., Experimental and Numerical Assessment of the Equivalent-Orthotropic-Thin-Plate model for Bending of Corrugated Panels, Int. J. Solid. Struct. 2017, 108, 11-23.
[65] Pipes R.B., Pagano N.J., Interlaminar stresses in composite laminates under uniform axial extension, J. Compos. Mater., 1970, 4, 538.
[66] Hsu P.W., Herakovich C.T., Edge effects in angle-ply composite laminates, J. Compos. Mater., 1977, 11(4), 422-428.
[67] O'Brien T.K., Characterization of delamination onset and growth in a composite laminate, in: K. Reifsnider, Ed.), Damage in Composite Materials: Basic Mechanisms, Accumulation, Tolerance, and Characterization, West Conshohocken, PA: ASTM Int., 1982, 140-167.
[68] Wang S.S., Choi I., Boundary-layer effects in composite laminates: Part 2 - free-edge stress solutions and basic characteristics, J. Appl. Mech., 1982, 49(3), 549-560.
[69] Whitcomb J., Raju I.S., Superposition method for analysis of free-edge stresses, J. Compos. Mater., 1983, 17(6), 492-507.
[70] Kress G., Width influence on stiffness measurements of multidirectional CFRP laminates under uniaxial load, Compos. Eng., 1992, 2(2), 83-90.
[71] Kress G., Free-edge influence on CFRP-laminate strength, Int. J. Damage Mech., 1994, 3, 194-211.
[72] Becker W., Closed-form solution for the free-edge effect in crossply laminates, Compos. Struct., 1993, 26(1-2), 39-45.
[73] Becker W., Kress G., Stiffness reduction in laminate coupons due to free-edge effect, Compos. Sci. Technol., 1994, 52, 109-115.
[74] Mittelstedt C., Becker W., Free-edge effects in composite laminates, Appl. Mech. Rev., 2007, 60(5), 217-245.
[75] Dhanesh N., Kapuria S., Achary G.G.S., Accurate prediction of three-dimensional free edge stress field in composite laminates using mixed-field multiterm extended kantorovich method, Acta Mech., 2016, 228(8), 2895-2919.
[76] Hajikazemi M., Paepegem W.V., A variational model for free-edge interlaminar stress analysis in general symmetric and thin-ply composite laminates, Compos. Struct., 2018, 184, 443-451.
[77] Seydel E., Über das Ausbeulen von rechteckigen, isotropen oder orthogonal-anisotropen Platten bei Schubbeanspruchung, Ingenieur-Archiv, 1933, 4(2), 169-191.
[78] ANSYS® Academic Research, Release 19.2.
[79] MATLAB®, Release 2019a.
[80] Winkler M., Analysis of Corrugated Laminates, 3407, ETH Zürich, diss. ETH No. 20130, 2012.
[81] Whitney J.M., Analysis of anisotropic laminated plates subjected to torsional loading, Compos. Eng., 1993, 3(6), 567-582.
[82] Honickman H., Johrendt J., Frise P., On the torsional stiffness of thick laminated plates, J. Compos. Mater. 2014, 48(21), 2639-2655.

A Inner solutions

Table A1: Inner solutions

c	A/D	alu		$[0_4]$		$[90_4]$		$[\pm 45]_s$	
0	A_{11}	76923		290842.9		5014.5335		79992.3	
	A_{22}	76923		5014.53		290842.94		79992.3	
	A_{66}	26923		5000.0		5000		72936.4	
	D_{11}	6410.3		24236.9		417.8778		6666.03	
	D_{16}	–		–		–		4466.07	
	D_{22}	6410.3		417.8778		24236.9		6666.03	
	D_{26}	–		–		–		4466.07	
	D_{66}	2243.6		416.6667		416.6667		6078.03	
		CF	FE	CF	FE	CF	FE	CF	FE
5	A_{11}	71894.0	**71894.0**	297678.	**297678.**	5132.37	**5132.80**	19618.0	**19576.4**
	A_{22}	467.345	**467.282**	30.4657	**30.4616**	1767.01	**1728.63**	485.992	**478.248**
	A_{66}	26222.9	**26222.9**	4871.13	**4871.12**	4871.13	**4871.22**	71056.5	**71052.9**
	D_{11}	960705.	**961309.**	3977805	**3980300**	68582.9	**68625.0**	262151.	**262790.**
	D_{22}	6245.03	**6244.99**	407.107	**407.104**	23612.2	**23581.9**	6494.21	**6491.89**
	D_{66}	2302.94	**2530.85**	427.690	**470.016**	427.690	**469.711**	6238.84	**6849.36**
25	A_{11}	109957.	**109957.**	455531.	**455531.**	7853.98	**7855.93**	29462.6	**29452.5**
	A_{22}	13.0571	**13.0558**	0.851180	**0.85094**	49.3684	**48.5100**	13.5781	**13.4556**
	A_{66}	17139.7	**17142.0**	3183.10	**3183.52**	3183.10	**3183.52**	46432.7	**46416.6**
	D_{11}	34366000	**34375300**	142372440	**142410000**	2454697	**2455880**	9208302	**9219390.0**
	D_{22}	4080.90	**4080.81**	266.029	**266.024**	15429.7	**15296.3**	4243.73	**4233.50**
	D_{66}	3524.21	**7001.42**	654.498	**1300.27**	654.498	**1300.26**	9547.35	**18945.00**